Environmental Technology & Innovation 31 (2023) 103149

Contents lists available at ScienceDirect

Environmental Technology & Innovation

journal homepage: www.elsevier.com/locate/eti

Application of nanocomposites in integrated photocatalytic techniques for water pollution remediation

R. Suresh [a], Lalitha Gnanasekaran [a,b], Saravanan Rajendran [a,c,*], Matias Soto-Moscoso [d], Wei-Hsin Chen [e,f,g], Pau Loke Show [h], Kuan Shiong Khoo [i,**]

[a] Departamento de Ingeniería Mecánica, Facultad de Ingeniería, Universidad de Tarapacá, Avda. General Velásquez 1775, Arica, Chile
[b] University Centre for Research & Development, Department of Mechanical Engineering, Chandigarh University, Mohali, Punjab, 140413, India
[c] Department of Chemical Engineering, Lebanese American University, Byblos, Lebanon
[d] Universidad Autónoma de Chile, Chile
[e] Department of Aeronautics and Astronautics, National Cheng Kung University, Tainan 701, Taiwan
[f] Research Center for Smart Sustainable Circular Economy, Tunghai University, Taichung 407, Taiwan
[g] Department of Mechanical Engineering, National Chin-Yi University of Technology, Taichung 411, Taiwan
[h] Department of Chemical Engineering, Khalifa University, Shakhbout Bin Sultan St - Zone 1, Abu Dhabi, United Arab Emirates
[i] Department of Chemical Engineering and Materials Science, Yuan Ze University, Taoyuan, Taiwan

ARTICLE INFO

Article history:
Received 28 February 2023
Received in revised form 9 April 2023
Accepted 10 April 2023
Available online 18 April 2023

Keywords:
Organic pollutants
Photocatalysis
Nanocomposites
Water treatment
Integrated technologies

ABSTRACT

In recent years, photocatalysis integrated with other water purification technique is emerging to decontaminate the polluted water effectively. Herein, a focus on adsorptive photocatalysis, photo-Fenton, photo–electrocatalysis, photocatalytic ozonation, sono-photocatalysis and photo–piezocatalytic techniques developed for degradation of organic water pollutants has been provided. Specifically, application of nanocomposites in the degradation of different organic pollutants (dyes, pesticides, antibiotics, phenolic compounds etc.,) via integrated photocatalysis was reviewed. The catalytic performances of different nanocomposites along with the experimental parameters such as dosage, light source, irradiation time, pollutant' concentration was summarized. Photocatalysis integrated with multiple techniques was also introduced. Current challenges, future perspectives and conclusion of this literature survey have been briefed. Researchers who are working in photocatalytic water treatment might be benefited by this review.

1. Introduction

Water is a vital resource for living beings including human, animals and plants. Anthropogenic activities such as domestic sewage disposal, industrial effluents, landfill leachates and release of different toxic and hazardous chemical substances (contaminants) into the natural water ecosystems including river, ocean and ground water are of serious concern in the world (Mahabeer and Tekere, 2021; Jakobczyk-Karpierz and Slosarczyk, 2022). Water contaminants may

* Corresponding author at: Departamento de Ingeniería Mecánica, Facultad de Ingeniería, Universidad de Tarapacá, Avda. General Velásquez 1775, Arica, Chile.
** Corresponding author at: Department of Chemical Engineering and Materials Science, Yuan Ze University, Taoyuan, Taiwan.
E-mail addresses: saravanan3.raj@gmail.com (S. Rajendran), kuanshiong.khoo@saturn.yzu.edu.tw (K.S. Khoo).

https://doi.org/10.1016/j.eti.2023.103149

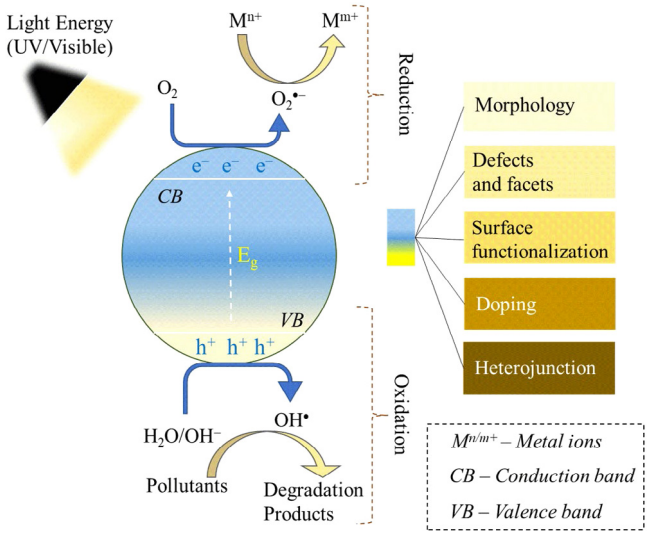

Fig. 1. Photocatalytic mechanism for decontamination/detoxification of organic/inorganic pollutants in water.

be inorganic, organic or organometallic substances. Heavy metal ions (e.g., mercury, lead)/metalloids (arsenic) (Chen et al., 2023a; Lucero Rincon et al., 2023) and anions (e.g., nitrate, sulphate) (Lenz et al., 2019; Karjalainen et al., 2021) are being inorganic water contaminants, whereas dyes (e.g., Remazol Gelb–GR, Eriochrome Black T), antibiotics (e.g., amoxicillin, oxytetracycline), and personal care products are some types of organic contaminants (De et al., 2022; Köktürk, 2022; Krishnan et al., 2021; Li et al., 2023a). Heavy metal complexes and organometallic compounds are also showing high environmental toxicity (Cuprys et al., 2018; Henriques et al., 2013). For the past decade, much attention was provided for the treatment of contaminated water resources (Ly et al., 2023). Physical (filtration, adsorption), chemical (neutralization, precipitation, reduction and advanced oxidation process) and biological (phytoremediation, aerobic/anaerobic degradation) water treatments were developed (Saleh et al., 2020; Okpara et al., 2023). Some treatments have advantages including portable, reliable, and cheaper, while there are downsides including need of high energy, toxic reagents, inadequate pollutant' removal efficiency and high operative expenditure. Among others, advanced oxidation processes are versatile wastewater purification techniques which can produce active species including hydroxyl ($^{\bullet}OH$), superoxide anion ($O_2^{\bullet-}$), and sulphate ($SO_4^{\bullet-}$) radicals upon irradiation of ultrasound wave, ultraviolet (UV) or visible light, electricity, and reagents (Saravanan et al., 2022). Active species hit organic and organometallic contaminants and degrade them in water.

Photocatalysis, an advanced oxidation process, has wide interest among the researchers, owing to its favourable merits such as possibility for mineralization of pollutants, utilization of solar light, and operation under mild conditions (Lu et al., 2022a; Saian et al., 2022). Photocatalysis is a catalytic process which occurs by absorption of light energy (UV–visible–near infrared) by the semiconductors or plasmonic photocatalysts (Kumar et al., 2022). Appropriate light energy excites the electrons from the valence band to the conduction band of semiconductor. The electrons and holes react with oxygen and water molecules and produce $O_2^{\bullet-}$ (reduction) and $^{\bullet}OH$ radicals (oxidation) respectively. Organic pollutants can be oxidatively degraded or mineralized by $^{\bullet}OH$ radicals, while the toxicity of inorganic pollutants can be minimized via photoreduction (Fig. 1). But, the life span of photogenerated charges is not high and thus photocatalysis exhibits low or inadequate degradation efficiency. Insufficient utilization of solar energy, and stability are also major drawbacks of photocatalytic water treatment. To avoid these demerits, different improvement tactics were reported (Fig. 1). Doping of metal/non-metal ions into the semiconductor photocatalysts is studying well due to its electron trapping capacity, reduction of band gap and surface defects. Importantly, optimum level of doping can lead better photocatalytic performance (Vaya and Surolia, 2020). Alternatively, nanocomposite-based photocatalysts were extensively developed for remediation of water pollution. But pollutant degradation efficiency is still not sufficient (Liu et al., 2022a, 2023) and thus an integration of the photocatalysis with other water purification techniques has been proposed. The integrated photocatalysis might eliminate the drawbacks of the component techniques.

In the review, the application of nanocomposites in integrated photocatalysis were discussed. Particularly, a discussion on various integrated photocatalytic technologies such as adsorptive photocatalysis, photo-Fenton, photo-sonocatalysis, photo–electrocatalysis, photo-ozonation, photo–piezocatalysis was provided. In addition, evaluation on their respective disclosed notable synergistic effects that can improve the performance of nanocomposite-based photocatalysts were evaluated. To ease readers understanding, a section consisted of researcher opinions and arising challenges on these integrated photocatalytic technologies were also provided.

2. Nanocomposites in photocatalytic water treatment

A single photocatalytic semiconductor (n- or p-type) could not accomplish the required performance in the wastewater treatment (Bayan et al., 2021). But heterostructures or nanocomposite (composed of two or more number of photocatalytic materials) will act as a good photocatalyst, owing to their charge separation capacity, resistance against photo-corrosion, and visible light harvesting tendency. The choice of photocatalytic components is depending on their valence/conduction band potentials, and band gap energy. Based on the semiconducting type, binary (p-n, p-p and n-n) and tertiary (n-p-n and p-n-p) nanocomposites, fabricated for water treatment are discussed below.

(a) n-n type

The n-n nanocomposite is constructed by coupling two n-type semiconductors. For example, Sabzehmeidani et al. (2020) have fabricated CeO_2/CdS n-n nanocomposite by using electrospinning technology. It possess good photocatalytic property towards degradation of rose Bengal under blue LED irradiation. A NH_2-UiO-66 (Zr)/perylene diimide n-n nanocomposite with 99.5% Cr(VI) reduction efficiency (irradiation time = 120 min) has also been reported (Ren et al., 2022). Recently, $BiOIO_3$/BiOBr n-n nanocomposite was developed for photocatalytic decomposition of tetracycline (Kuang et al., 2023). Within 80 min of visible light illumination, 74.91% tetracycline degradation efficiency was achieved for $BiOIO_3$/BiOBr.

(b) p-p type

The p-p type-nanocomposite is a prepared by integrating two p-type semiconductors. Recently, p-p type-nanocomposite was synthesized by coupling BiOBr and $Bi_{12}O_{17}Br_2$ nanoparticles which showed 99% sulfamethoxazole (20 ml, 20 mg l^{-1}) degradation efficiency (Wang et al., 2022a).

(c) p-n type

Compared to p-p and n-n, p-n nanocomposites have much attention in wastewater treatment. The p-n nanocomposite is prepared by coupling one n-type and p-type semiconductors. For instance, n-type CeO_2/p-type BiOI flower-like nanocomposite with higher Rhodamine B and methyl orange photocatalytic efficiency were reported (Song et al., 2018). Wang et al. (2019a) have reported Ag_3PO_4/$NaTaO_3$ p-n nanocomposite for the decomposition of rhodamine B in presence of visible light illumination.

(d) n-p-n type

The n-p-n type composite is constructed by using two n-type and one p-type semiconductors. For example, $Bi_4O_5I_2$/$Bi_2O_2CO_3$/BiOCl $_{0.8}I_{0.2}$ *n-p-n* nanocomposite photocatalyst with 99% of rhodamine B degradation efficiency (time = 60 min, light = 500 W Xe lamp) was reported (Sun et al., 2021). A visible-light active CeO_2/PPy/ZnO *n-p-n* nanocomposite with better photocatalytic capability towards decomposition of chlorophenol (efficiency = 92%; irradiation time = 180 min) was also demonstrated (Rajendran et al., 2022). Cu_2O/ZnO/Ag_3PO_4 p-n-n heterojunction, synthesized by co-precipitation approach was applied in the photocatalytic decomposition of (81.1%) methyl orange (Taddesse et al., 2020). A solvothermal synthesis method was reported for the preparation of Cu_3P/$ZnSnO_3$/g-C_3N_4 p-n-n heterojunction which showed good tetracycline (98.45%) and ciprofloxacin (87.57%) photocatalytic decomposition efficiency (Guo et al., 2021).

(e) p-n-p type

The p-n-p type-nanocomposite is synthesized by coupling two p-type and one n-type semiconductors. For instance, Ag_2CO_3/BiOI/$CoFe_2O_4$ p-n-p heterojunction was reported for the removal of elemental mercury under fluorescent light (Wang et al., 2019b). Both BiOI and $CoFe_2O_4$ has p-type property, while Ag_2CO_3 possess n-type property. Recently, $CoFe_2O_4$/$CoFe_2S_4$/$MgBi_2O_6$ *p-n-p* heterojunction with 82.7% cefotaxime sodium degradation efficiency (irradiation time = 60 min) was also reported (Wang et al., 2022b).

It should be mention that nanocomposites with different photocatalytic mechanisms were determined. Particularly, type-I, type-II, Z-scheme and S-scheme mechanisms were discussed below (Rani et al., 2023).

(a) Type-I

Type-I nanocomposite is composed by which the conduction band and valence band potential of one semiconductor is more positive and negative than those of another semiconductor. Wang et al. (2022c) have prepared ZnO/Co_3O_4 composite which showed type-I photocatalytic mechanism. However, type-I nanocomposite shows not enough charge separation efficiency since photoexcited holes and electrons are migrated in one direction that leads facile charge recombination.

(b) Type-II

In type-II nanocomposite, photoexcited electrons from conduction band and holes from valence band are migrated in the opposite direction between two semiconductors. It considerably avoids the charge recombination and thus generally exhibit good photocatalytic property.

(c) Z-scheme

In Z-scheme nanocomposite, the light induced electrons and holes in different semiconductor will reacts with electron acceptor and donor respectively. The retained electron present in the lower conduction band of semiconductor will be neutralized with the holes present in valence band of another semiconductor. Consequently, an effective charge separation efficiency is obtained. For example, Chen et al. (2023b) have reported g-C_3N_4/Ag_3PO_4 Z-scheme nanocomposite for the degradation of ofloxacin (efficiency = 71.9%; time = 10 min). Another Z-Scheme $La_2Ti_2O_7$/Ag_3PO_4 nanocomposite has also been reported for the degradation of rhodamine B, chloroquine phosphate, tetracycline, and phenol under sunlight irradiation (Chen et al., 2023c).

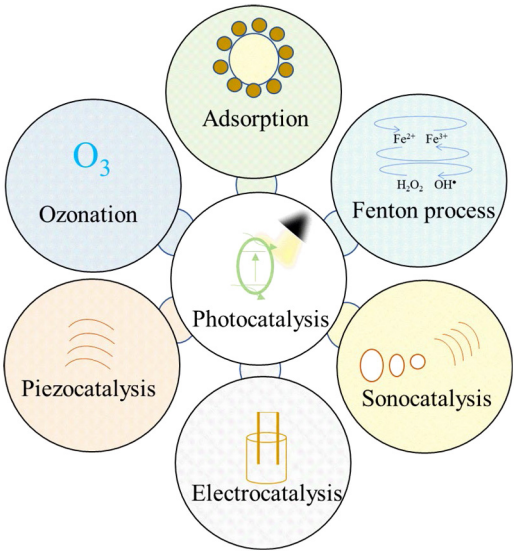

Fig. 2. Integrated photocatalytic techniques for wastewater treatments.

(d) S-scheme

S-scheme $Ti_{0.7}Sn_{0.3}O_2$/g-C_3N_4 nanocomposite was prepared by coupling $Ti_{0.7}Sn_{0.3}O_2$ and g-C_3N_4 semiconducting materials (Guo et al., 2022). This nanocomposite shows 98.5% Rhodamine B (irradiation time = 20 min) and 88.3% tetracycline (irradiation time = 40 min) degradation efficiency. Tetracycline hydrochloride was also decomposed by $CoFe_2O_4$/$NiFe_2O_4$ S-scheme nanocomposite photocatalyst (Song et al., 2023). About 76.1% removal efficiency was reported within 60 min of irradiation.

It is important to mention that the application of nanocomposites in photocatalytic water treatment is extensive. Consequently, critical reviews have also been published in recent years. For examples, cellulose based nanocomposites with photocatalytic activities have been reviewed by Sudhaik et al. (2023). The photocatalytic properties of zinc derived nanocomposites including metals or non-metals or polymers/Zn-derived nanocomposites have been reviewed by Rani et al. (2023). A review on TiO_2/carbon materials (graphene and its derivatives, g-C_3N_4, activated carbon etc.,)-based composite photocatalysts with their water pollutants degradation tendency were published (Thambiliyagodage, 2022). Also, adsorption coupled photocatalytic performances of g-C_3N_4-based composites were elaborately discussed in another review (Yu and Huang, 2023). Masekela et al. (2023) have concentrated on piezo-photocatalytic elimination of organic contaminants (organic dyes and pharmaceuticals) and bacteria from water by using $BaTiO_3$-based nanomaterials. However, reviews on application of nanocomposites in integrated photocatalytic technologies for removal of water contaminants is quite rare. Hence, this review has written with main focus on different integrated photocatalytic techniques with special attention to nanocomposite-based catalysts.

3. Integrated photocatalytic techniques

Fig. 2 illustrates the different integrated photocatalytic techniques such as adsorptive photocatalysis, photo-Fenton technique, photo-sonocatalysis, photo–electrocatalysis, photo-ozonation and photo–piezocatalysis.

3.1. Adsorptive photocatalysis

Adsorption is a versatile technique which can remove multiple types of pollutants including organics, heavy metal ions, metalloids from water. The drawback of adsorption technique is that it cannot degrade and/or mineralize the organic pollutants. Further, the regeneration process is essential for reuse of adsorbents and this additional process will be costlier. Whereas photocatalysis integrated with adsorption (adsorptive photocatalysis) is an effective technique since it can instantaneously adsorb and degrade pollutants. In photocatalysis, the pollutant molecules which contact with the surface of the photocatalyst can only undergo degradation. Thus, photocatalysts with huge adsorption ability could show best degradation efficiency. For an effective adsorptive photocatalysis, photocatalyst is combined with adsorbent materials. The adsorbent with huge surface area is employed as a support matrix to evenly disperse the photocatalyst. Selection of adsorptive component is important, since a usual adsorbent does not exhibit photocatalytic activity, and therefore the performance of photocatalyst-adsorbent system will be comparatively low. On the other hand, the adsorptive components such as graphene could decrease the recombination rate of photo-charges, produced by semiconductor photocatalysts.

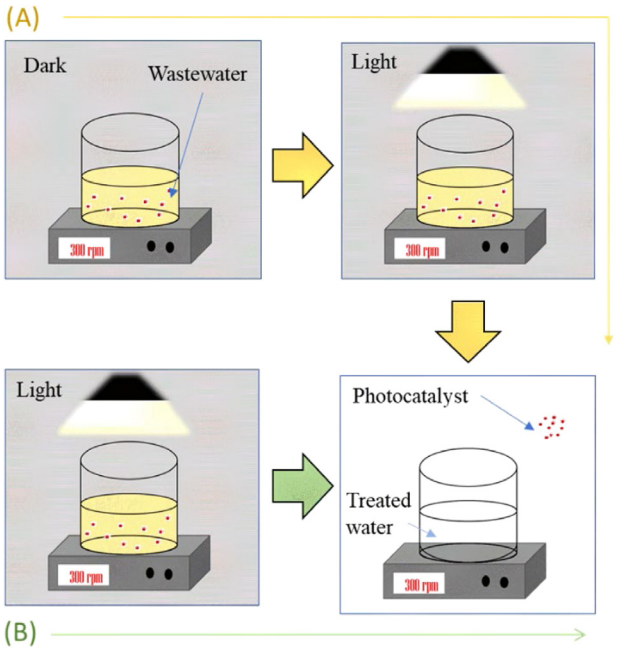

Fig. 3. Experimental procedure for an adsorptive photocatalysis: (A) Adsorption in dark followed photocatalysis and (B) simultaneous adsorption and photocatalysis.

Adsorptive photocatalytic experiments are performed by adsorption followed by photocatalytic process or instantaneous adsorption-photocatalytic process (Fig. 3). Generally, an adsorption experiment is initially performed in dark (contact time = 30 min) and then the reaction mixture is exposed to light irradiation with suitable wavelengths. Alternatively, the aqueous dispersion consists of pollutant and the photocatalyst is irradiated by light sources (Yu et al., 2022). No dark adsorption experiment is performed. Light irradiation time is varied according to the photocatalyst and molecular structure of pollutants.

Table 1 evaluates the binary nanocomposites-based adsorptive photocatalysts and their performances in pollutant removal. It should be clear that the adsorptive component will be carbon materials (GO, RGO), polymers (alginate) or even other photocatalytic materials. The degradation efficiency of a particular pollutant is mainly dependent on the components of a nanocomposite.

Binary nanocomposites consisting of one modified photocatalyst have also been reported. For instance, Song et al. (2022) have adopted a pyrolytic route to prepare phosphoric acid (H_3PO_4)-modified TiO_2/biochar composite. First, porous biochar with a specific surface area of 1747.8 m^2 g^{-1} was synthesized from jute fibres (450 °C). H_3PO_4-modified TiO_2/biochar composite (optimized dosage = 0.6 g L^{-1}) was initially utilized to capture Congo red or methylene blue (100 mL,) and subsequently subjected to photocatalytic process (light source: 500 W Xe-lamp, intensity = 1500 mW cm^{-2}) for degradation of adsorbed dyes. The adsorption capacity of this composite is reported as 223.4 and 208.9 mg g^{-1} (temperature = 30 °C) for methylene blue and Congo red respectively. A complete degradation of adsorbed dyes was reported. Importantly, the spent nanocomposite was regenerated and reused five times with good removal rates (88.1–69.3%). Lignin-derived biochar consists of BiOBr nanoparticles with oxygen vacancies were prepared for elimination of rhodamine B from water (Yang et al., 2023). Biochar induced oxygen vacancies in BiOBr nanoparticles and thus BiOBr nanoparticles obtained improved visible-light absorption capacity (band gap = 2.56 eV), and effective separation of photo-charges. Consequently, 99.2% of rhodamine B was removed by BiOBr/biochar in presence of visible-light irradiation (60 min) which is greater (54.5%) than that of pure BiOBr nanoparticles. Based on the electron paramagnetic resonance spectroscopy and radical trapping experiments, it was determined that the superoxide anion radical ($O_2^{\bullet -}$) are the active species for degradation of dye molecules.

Ternary nanocomposites were also evaluated as adsorptive photocatalysts. As an example, Ag_3PO_4/RGO/$CoFe_2O_4$ nanocomposite was prepared by precipitation–deposition method and used for elimination of levofloxacin from aqueous medium through adsorptive photocatalysis technique (Hu et al., 2021). This ternary composite displayed 90.7% levofloxacin removal efficiency which is higher than that of single components. RGO played as adsorbent and photocharge trap centre that boosts the charge separation efficiency of this nanocomposite. Levofloxacin removal was achieved within 0.5 and 1.0 h for adsorption and photocatalysis respectively. The light source, catalyst dosage, and concentration of levofloxacin was 30 W LED lamp, 0.1 g and 10 mg L^{-1} (100 mL) respectively. Singlet oxygen has a significant role in levofloxacin degradation by the Ag_3PO_4/rGO/$CoFe_2O_4$/visible light system. Singlet oxygen was formed by reaction

Table 1
Pollutant removal performance of some recently reported binary nanocomposites via adsorptive photocatalysis.

Adsorptive photocatalyst	Pollutants	Concentration of pollutant (volume)	Dosage (mg)	Adsorption time (stirring in dark)	Light source	Light illumination time (min)	Efficiency (adsorptive photocatalysis)	Reference
Molybdenum disulphide (MoS_2)/Titanium dioxide (TiO_2)	Methylene blue Crystal violet	25 mg L^{-1} (50 mL)	25	30 min	300 W lamp	1 h	100% 100%	Chandrabose et al. (2021)
Bi_2WO_6/ protonated g-C_3N_4/polyamide membrane	17β-estradiol	3 mg L^{-1} (40 mL)	Membrane	3 h	300 W Xe-lamp	240	99.5%	Qing et al. (2022)
$Bi_4O_5I_2$/BiOI	Malachite green	120 mg L^{-1} (50 mL)	20	30 min	500 W Xe-lamp	120	100%	Ding et al. (2023)
CdS/porous geopolymer	Methylene blue Crystal violet Rhodamine B Methyl orange	20 mg L^{-1}	1:25 (solid–liquid ratio)	30 min	350 W Xe-lamp	100	86.17%	Ji et al. (2022)
CuO/ activated carbon	Amoxicillin	100 mg L^{-1}		60 min	Sunlight	90	98%	Yahia et al. (2022)
Graphene oxide (GO)/ cerium oxide (CeO_2)	Doxorubicin	0.5 mM (3 mL)	1 mg mL^{-1}		9 W LED lamp	420	99.8%	Abbasi et al. (2022)
Carbonized manganese-crosslinked sodium alginate	Cr(VI) As(III) As(V)					45	>98%	Mao et al. (2022)
Reduced graphene oxide (RGO)/zinc Oxide (ZnO) + 2 mL 30% H_2O_2	Chloramphenicol	1.0 g L^{-1} (40 mL)	0.1 g	30 min	4 W UVP compact lamp	40	91%	Sodeinde et al. (2022)
Co_3O_4/WO_3	Ethylparaben Methylene blue	10 mg L^{-1}	30	10 min sonication + 30 min	300 W Xe-lamp	15	88% 100%	Ngigi et al. (2019)
TiO_2/Ag_3PO_4	Rhodamine B Methylene blue	6 mg L^{-1} 8 mg L^{-1} (200 mL)	0.5 g L^{-1}	30 min	300 W Tungsten halogen-lamp	6 4	98% 99.1%	Nyankson et al. (2021)
β-cyclodextrin/Cu_2O	Tetracycline Methylene orange Congo red	50 mg L^{-1}(100 mL)	25	–	1000 W Xe-lamp	30	97% 84% 93%	Wang et al. (2023)
Polyvinyl alcohol/CuO	Caffeine	50 mg L^{-1}(100 mL)	30	60 min	Visible light	80	96.55%	Dileep Kumar et al. (2023)
Bismuth Molybdate (Bi_2MoO_6)/ Reduced Graphene Oxide	Naphthalene	50 mg L^{-1}(100 mL)	30	30 min	250 W UV–vis light	60	95%	Maswanganyi et al. (2021)
$Bi_2O_2CO_3$/ biochar	Tetracycline	70 mg L^{-1} (100 mL)	60	30 min	300 W Xe-lamp	60 min	84.7%	Luo et al. (2023)
Polyaniline/TiO_2	2,4-dichlorophenoxyacetic acid Triclopyr acid	10 mg L^{-1}	0.5 g L^{-1}	30 min	125 W Hg-lamp	120 min	99.91% 90.72%	Moradeeya et al. (2022)

between photo-generated holes and $O_2^{\bullet-}$ radical. Liu et al. (2021) have reported the preparation of polyaniline/dicarboxyl acid cellulose/GO composite for the degradation of reactive brilliant red K-2G. The morphology and dispersion of the nanocomposite was influenced by dicarboxyl acid cellulose. Only 25 min was needed for completion of dye adsorption (adsorption capacity = 447.0 mg g^{-1}), whereas removal capacity increased as 729.0 mg g^{-1} (efficiency = 97.5%) by photocatalysis (180 min). The instantaneous adsorption-photocatalytic technique leads to the removal capacity of 733.3 mg g^{-1} (efficiency = 97.9%). Li et al. (2022a) have synthesized visible light active TiO_2/carbon nanosheets/SiO_2 for

degradation of chlorpromazine via adsorptive photocatalysis. Single photocatalysis and adsorptive photocatalysis shows 91.1% and 94.2% chlorpromazine degradation efficiency respectively. The better activity of ternary composite is due to increased chlorpromazine adsorption on carbon nanosheets/SiO_2 particles. The $O_2^{\bullet-}$ radical is found to have a key role in chlorpromazine degradation. Importantly, the treated water has negligible toxicity. Yu et al. (2022) found that TiO_2/Zr-doped SiO_2/g-C_3N_4 composite possesses good degradation activity towards the targeted antibiotic under 300 W Xe-lamp light (150 mW cm^{-2}). The degradation efficiency for berberine hydrochloride, oxytetracycline and tetracycline was obtained as 98.11, 84.84 and 80.76%, respectively. The adsorption capacity of Zr-doped SiO_2 and photocatalytic ability of TiO_2/g-C_3N_4 favours the antibiotic degradation performance. In another paper, ZnO/cobalt oxide (CoO_x)/cerium oxide (CeO_2) nanocomposite with high degradation rate (98.8%) of Congo red via adsorptive photocatalysis was reported (Lu et al., 2022b). The optimized catalyst concentration, pH and contact time is 1 g L^{-1}, 6-7 and 65 min respectively. The nanocomposite exhibited better adsorption and photocatalytic performance than single components. Lin and Tseng (2022) have prepared ferric oxide (Fe_3O_4)/silver (Ag)/$TiO_{2-x}N_x$ core–shell (core = Fe_3O_4/Ag; shell = $TiO_{2-x}N_x$) nanocomposite with good adsorptive photocatalysis towards methylene blue degradation. The nanocomposite heated at 400 °C (2 h under nitrogen atmosphere) displays an adsorption and photocatalytic degradation efficiency of 54.8 and 25.1% respectively towards methylene blue degradation.

3.2. Photo-Fenton technique

Fenton process involves the generation of hydroxyl (•OH) radicals by the reaction between Fe^{2+} ions and hydrogen peroxide (H_2O_2) under low pH (acidic) conditions. It has merits such as a simple operation process, and cost effectiveness. Iron compounds such as ferric oxide (Fe_2O_3), Fe_3O_4, copper ferrite ($CuFe_2O_4$), iron oxyhydroxide (FeOOH) were employed in the heterogeneous Fenton process for wastewater purification purposes. Nevertheless, the Fe^{3+} reduction is slow which limits the catalytic process. It also needs high acidic conditions and generate sludge in huge quantity. These problems are expected to solve by integrating Fenton process with photocatalysis. Photo-Fenton catalytic experiment is conducted in a photoreactor. Appropriate concentration of the photo-Fenton catalyst should be added into reactor containing aqueous solution of pollutants and the set-up is kept under magnetic stirring. The dispersion is stirred under dark for certain time period (usually for 30 min). After that, certain amount of H_2O_2 is added into the reaction mixture, and then lamp is switched on. Samples were collected at regular time interval and analysed through UV–visible and/or high-performance liquid chromatography. Many studies showed that the integration of Fenton process and photocatalysis (binary nanocomposites) could enhance the charge separation efficiency and provide electrons for Fe^{3+} reduction process ($Fe^{3+} \rightarrow Fe^{2+}$), therefore generating more active species for degradation of organic pollutants. Table 2 demonstrates the degradation efficiency under different catalyst prior to Photo-Fenton catalytic activity of binary nanocomposite.

Particularly, the optimum concentration of H_2O_2 is vital for the better photo-Fenton activity of the catalyst. For instance, rhodamine B was completely removed within 20 min in presence of 100 μL H_2O_2/Ag_3PO_4/CuO/visible light system (Ma et al., 2017). But the activity of Ag_3PO_4/CuO/visible light systems is less in presence of 50 μL H_2O_2. The degradation efficiency decreases and the time increases when the concentration of H_2O_2 is greater than 150 μL. It is because of formation of $HO_2^{\bullet}$ and O_2 by the reaction between excessive H_2O_2 and •OH.

Likewise iron ions, Cu ions in copper oxide particles can will also generate •OH radicals from H_2O_2 as shown in the Eq. (1) and Eq. (2) below (Ma et al., 2017):

$$\equiv Cu(II) + e^- \rightarrow \equiv Cu(I) \quad (1)$$

$$\equiv Cu(I) + O_2 \rightarrow \equiv Cu(II) \quad (2)$$

Ternary nanocomposites were developed to utilize in photo-Fenton integrated process. For instance, Fe-doped g-C_3N_4/reduced graphene hydrogel/visible light/H_2O_2 system was developed for the treatment of phenol and coking wastewater (TOC = 25.3 mg L^{-1}) (Hu et al., 2020b). Fe-doped g-C_3N_4/reduced graphene (10%) hydrogel showed highest rate constant (k = 0.0948 min^{-1}) and stability than pure g-C_3N_4 or Fe-doped g-C_3N_4 catalysts. This system also showed good degradation efficiency towards coking wastewater (recyclability = 7). The photo-induced electrons accelerate Fe^{3+}/Fe^{2+} process and of H_2O_2 decomposition. Graphene transfers the electrons and convert H_2O_2 in to •OH radical. Overall, a huge quantity of •OH radicals were generated, which greatly improve the degradation efficiency. CdS/CuS/g-C_3N_4 nanocomposite has been applied as photo-Fenton catalyst for the degradation of methyl orange (Xu et al., 2023). It exhibited increased light absorption tendency and the active centres. About 96% methyl orange degradation efficiency was reported under visible light irradiation for 35 min illumination (k = 0.088 min^{-1}). It retains 86% efficiency even after fifth cycle. The improved activity is primarily attributed to the conversion and recycling of Cu^{2+} and Cu^+. RGO containing Fe_2O_3 and TiO_2 nanoparticles was prepared for the degradation of methyl orange (Zheng et al., 2022). In presence of light from light-emitting diode lamp (λ = 420 nm, 5 W) and H_2O_2 (19.8 mmol L^{-1}), this composite showed complete degradation of methyl orange. The Fe_2O_3 nanoparticles act as Fenton reagent and photocatalyst. In the composite, the Fe leaching was controlled, thereby leading to the long lifetime of the composite. The performance of photo-Fenton process depends on the solution pH. It was reported that the phenol removal efficiency (at 30 min) of photo-Fenton process is 24.0, 83.5, and 93.9% at pH value of 11, 7, and 3, respectively (Hu et al., 2020b). Acidic pH is found to be suitable for the performance of photocatalysis-Fenton system. Alkaline pH is not favourable, since the surface adsorbed H_2O molecules are replaced by OH^-, which will not generate •OH radicals from H_2O_2.

Table 2
Photo-Fenton catalytic activity of binary nanocomposite in the degradation of pollutants in water.

Catalyst	Catalyst dosage	Pollutant	Adsorption–desorption equilibrium (min)	Photo-Fenton experiment	Degradation efficiency	Degradation time (min)	Reference
Slice g-C_3N_4/CdS	0.2 g L^{-1}	Rhodamine B, 10 mg L^{-1} (50 mL)	30	500 W Xe-lamp, 20 mg L^{-1} ferrous solution		16	Li et al. (2021a)
Ag_3PO_4/CuO	0.01 g	Rhodamine B, 1×10^{-5} mol L^{-1}(10 mL)	0.5 h	300 W Xe-lamp, [H_2O_2] = 100 μL	100%	20	Ma et al. (2017)
CeO_2/Fe_3O_4	1.0 g L^{-1}	Congo red, 1000 mg L^{-1}	120	[H_2O_2] = 3.75 mL L^{-1}	82%	120	Xiang et al. (2022)
Cu/$CuFe_2O_4$-oxygen Vacancies	10 mg	Phenol, 100 mg L^{-1} (30 mL)	30	[H_2O_2] = 40 μL	92.72%	18	Wang et al. (2022d)
Fe^{2+}/Fe^{3+} co-doped $BiVO_4$/Ag_3PO_4	20 mg	Tetracycline, 20 mg L^{-1} (100 mL)	30	Xe-lamp, 30% [H_2O_2] = 100 μL	99.70%	60	Zhang et al. (2023)
Fe_3O_4/schwertmannite	50 mg	Phenol, 100 mg L^{-1} (50 mL)	30	[30 wt% H_2O_2] = 45 μL	98%	10	Li et al. (2020a)
Surface oxygen vacancies enriched FeOOH/Bi_2MoO_6		Phenol (30 mL)	30	350 W Xe-lamp, H_2O_2	100%	3 h	Hu et al. (2020a)
Fe/α-Fe_2O_3	30 mg	Rhodamine B, 10 mg L^{-1} (60 mL)	60	300 W Xe-arc lamp, [H_2O_2] = 0.7 mL	96.5%	60	Feng et al. (2021)
g-C_3N_4/FeOCl	0.2 g L^{-1}	Rhodamine B, 20 mg L^{-1} (100 mL)	30	300 W Xe-lamp, H_2O_2	97%	9	Jiang et al. (2022)
Reduced graphene oxide/$CoFe_2O_4$	0.02 g L^{-1}	Basic red 46 Basic red 18, 20 mg L^{-1}, (500 mL)	30	150 W visible light, [H_2O_2] = 0.04 mM	88% 90%	210	Mazarji et al. (2021)
$SrWO_4$/MIL-88A(Fe)	10 mg	Methylene blue, (30 mL)	30	440 W metal halide-lamp, 30 wt% H_2O_2	93.75%	4	Wei et al. (2023)
δ-FeOOH/$BiOBr_{0.5}I_{0.5}$	0.02 g	Tetracycline, 50 mg L^{-1}, (80 mL)		300 W Xe-lamp, 10 mM H_2O_2	93%	1 h	Li et al. (2022b)
Fe_3O_4/α-FeOOH	75 mg	Tetracycline Hydrochloride, 10 mg L^{-1},	30	300 W Xe-lamp, 0.1 mL of H_2O_2 (10 mM)	100%	90	Huang et al. (2021)
Graphene quantum dots/α-FeOOH	50 mg	Ciprofloxacin, 10 mg L^{-1} (200 mL)	–	350WXe lamp, 0.50 mM H_2O_2	93.73%	60	Pervez et al. (2022)
Bacterial cellulose/pyrite (FeS_2)		Textile dye (direct black 22, direct red 23, direct red 227, reactive blue 21) solution, 15 mg L^{-1}, 200 mL	30	300 W Incandescent Lamp, 50 mg L^{-1} H_2O_2	96.82%	180	Santana et al. (2023)

3.3. Photo-sonocatalysis

Photo-sonocatalysis is a catalytic reaction that occurs by using ultrasound waves passing through a water medium. Ultrasound waves create active •H and •OH radical via homolytic cleavage of water molecules within the cavitation bubbles. These radicals are non-selectively hit by organic contaminants and transform into by-products in water medium. But it lacks complete mineralization of organic pollutants with less ultrasound irradiation times. On the one hand, an integration of sonocatalysis with photocatalysis has found a good strategy to overcome the drawbacks of the sole sonocatalysis. Table 3 shows a list of photo-sonocatalysts and their activity in pollutant' degradation reactions.

Major inferences observed from the photo-sonocatalysts activities are highlighted out as per below:

(a) Photo-sonocatalysis is effective in the degradation of organic molecules.
(b) By changing light wavelength and power of ultrasonic waves, the degradation performance of the catalysts can be altered.

Table 3
Some examples of photo-sonocatalysts with their activity.

Catalyst	Catalyst dosage	Pollutant	Light source	Ultrasound	Removal efficiency (%)	Degradation time (min)	Active species	Reference
$FeVO_4/BiVO_4$ + 20 mM H_2O_2	500 mg L^{-1}	Levofloxacin (20 mg L^{-1}, 100 mL)	Xe-lamp	Ultrasonic generator (40 kHz, 50 W)	98.91	60	•OH, and $O_2^{\bullet-}$ radicals	Fan et al. (2022)
TiO_2/Fe_3O_4/activated carbon	0.4 g L^{-1}	Tetracycline	6 W UV-C	Probe sonicator (20 kHz)	∼100.0	60	h^+, •OH radicals and $^1O_2$	Kakavandi et al. (2019)
Zinc–chromium layered double hydroxide/biochar	0.6 g L^{-1}	Rifampicin (15 mg L^{-1})	30 W LED lamp	Ultrasonic bath (150 W, 36 kHz)	98.0	40	•OH, h^+, and $O_2^{\bullet-}$ radicals	Rad et al. (2022a)
ZnCr layered double hydroxide/reduced graphene oxide	1.5 g L^{-1}	Rifampicin (15 mg L^{-1}, 100 mL)	LED lamp	Ultrasonic bath (150 W)	87.3	60	•OH, h^+, and $O_2^{\bullet-}$ radicals	Rad et al. (2022b)
NiCr layered double hydroxide/ biochar	1 g L^{-1}	Rifadi (15 mg L^{-1})	50 W LED light	Ultrasonic bath (150 W)	80.3	90	•OH radical	Rad et al. (2023)
Er^{3+}-CdS/MoS_2	125 mg L^{-1}	17β-estradiol (1000 μg L^{-1}, 100 mL)	500 W Xe-lamp	Ultrasonic bath (40 kHz, 50 W)	95.29	180	•OH radical	Du et al. (2022)
N/Ti^{3+} co-doped TiO_2/Bi_2WO_6	7.5 mg	Methylene blue (5 mg L^{-1}, 15 mL)	500 W Xe-lamp	Ultrasonic cleaner (35 kHz, 180 W)	99.00	50	$O_2^{\bullet-}$ radical	Sun et al. (2020)
N-doped TiO_2/Ti_3C_2	15 mg	Rhodamine B (20 mg/L, 30 mL)	500 W Xe-lamp	Ultrasound irradiation	98.1	25	$O_2^{\bullet-}$, •OH radicals and h^+.	Ding et al. (2021)
N, Fe co-doped TiO_2/SWCNT	0.7 g L^{-1}	Sulfathiazole (40 mg L^{-1}, 200 mL)	250 W LED lamp	Probe ultrasonicator (24 kHz)	100.0	90	$O_2^{\bullet-}$, and OH• radicals	Hayati et al. (2020)
ZnO/graphene oxide ZnO/carbon nanotube	0.05 g	4-Nitrophenol (10 mg L^{-1})	160 W Hg lamp, 5 ml H_2O_2	Titanium probe sonicator (60 W, 20 kHz)	100.0	180	OH• radicals	Khairy et al. (2020)
$Ti_3C_2T_x/Ni_xMg_{4-x}S_4$	50 mg	bisphenol A (10 mg L^{-1}, 50 mL)	250 W LED lamp	Ultrasonicator (970 kHz, 400 W)	∼92	60	Holes, OH•, and $O_2^{\bullet-}$ radicals	Vigneshwaran et al. (2020)
TiO_2-Pd/ pumice stone	0.5 g L^{-1}	ciprofloxacin (20 mg L^{-1}, 50 mL)	10-W LED lamp	Ultrasound bath (40 kHz, 300 W)	79.44%	120	•OH, $O_2^{\bullet-}$, and $HO_2^{\bullet}$ radicals	Motlagh et al. (2021)
Pt/CeO_2	0.2 g	Acid red 17 (50 mg/L, 80 mL)	250 W Hg-lamp	Sonicator (40 kHz)	95%	30	•OH, and $O_2^{\bullet-}$ radicals	Khan et al. (2022)
g-C_3N_4/Ni–Ti LDH	1.25 g L^{-1}	Amoxicillin (1.0 g L^{-1}, 100 mL)	500 W Hg-lamp	Ultrasound probe (20 kHz, 200 W)	99.5%	75	•OH radicals	Abazari et al. (2019)
Graphene/ cobalt ferrite ($CoFe_2O_4$)	0.99 g L^{-1}	Diazinon (10 mg L^{-1})	Hg-lamp	Ultrasound bath	100.0	100	hole and •OH radicals	Al-Musawi et al. (2022)

(c) Pollutant degradation time can be minimized.
(d) Active free radicals which are responsible for degradation reactions are dependent on the catalysts.

3.4. Photo–electrocatalysis

Numerous kinds of organic pollutants including dyes, pharmaceuticals were destroyed in water via electrocatalysis. In an electrocatalytic cell, nanocomposite modified anode generates hydroxyl radicals which will oxidize the organic pollutants. To improve the performance, photo–electrocatalytic technique was developed (Marinho et al., 2022). A schematic representation of a simple photo–electrocatalytic chamber is displayed as Fig. 4. It contains light source,

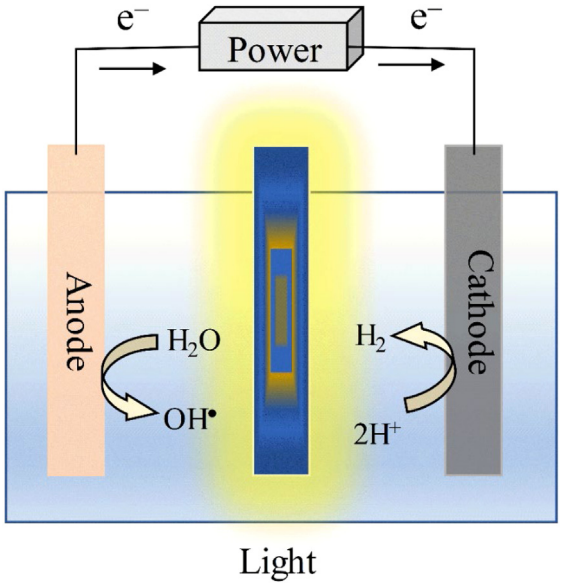

Fig. 4. Schematic representation of photo–electrocatalytic cell.

cathode, anode, electrolytes, electrocatalysts and powder source. Under the light irradiation, the applied external voltage will effectively separate the photogenerated electron–hole pairs (Li et al., 2023b).

Nanocomposite modified electrode for photo–electrocatalytic degradation processes were reported. For instance, $BiVO_4$/ZnO/FTO electrode was fabricated and employed in the photo–electrocatalytic degradation of tetracycline in (electrolyte = 0.1 M of Na_2SO_4) water (Li et al., 2021b). The light source and bias voltage are 300 W Xe-lamp and 1.6 V respectively. About 84.5% tetracycline degradation efficiency was obtained. It has been found that the ZnO nanorods effectively separated photoinduced charges, while ZnO/$BiVO_4$ nanostructures strongly absorbed the light and improved the mass transfer rate. Active species involved in this photo–electrocatalytic degradation process are $^{\bullet}O_2^-$ and $^{\bullet}OH$ radicals. Nitrogen-doped graphene quantum dots/reduced graphene oxide/carbon fabric displayed 93% methylene blue degradation efficiency at 2 V (Riaz et al., 2019). Porous structure of this composite makes it efficient in the degradation process. Ni–Mn layered double hydroxides/g-C_3N_4 nanocomposites modified glassy carbon electrode showed ≥99% rhodamine b degradation efficiency under visible light (Shakeel et al., 2019). Zn_2SnO_4/RGO/Ag/AgBr photo–electrocatalyst was reported for degradation of methylene blue (Peng et al., 2023). The Z-scheme mechanism generates $^{\bullet}OH$ and $O_2^{\bullet-}$ radicals which play a major role in methylene blue degradation. Carbon (graphene-like)/SnO_2/TiO_2 nanocomposite-based anode was fabricated for degradation of five pharmaceutical contaminants (e.g. chloramphenicol, bupropion, venlafaxine, carbamazepine and triclosan) (Kaur et al., 2021). This composite anode degraded 90% of the targeted pharmaceutical contaminants within 60 min. This is because of its high photocharge separation efficiency and active species producing capacity. Ju et al. (2021) have prepared fullerenes (C_{60})/AgCl/ZnAlTi layer double oxide nanocomposites coated platinum as working electrode for decomposition of bisphenol A via photo–electrocatalytic process. C_{60}/AgCl/ZnAlTi layer double oxide intensively absorbs in the near ultraviolet region. The photoelectrocatalytic degradation efficiency is reported as 99% under 300 W Xe-lamp irradiation (−1.0 eV).

3.5. Photo-ozonation

Ozone (O_3) is a prevailing oxidant and it is commonly used for the water purification process. However, ozone is an unstable molecule in an aqueous environment and it selectively degrades organic substances such as aromatic compounds (acidic conditions). Ozone is not entirely mineralizing the targeted organic molecules.

These demerits can be rectified by integrating it with photocatalytic techniques (photocatalytic ozonation). For example, g-C_3N_4/Fe-MCM-48 composite catalysts have been prepared and used in the photocatalytic ozonation of azithromycin (Ling et al., 2023). In presence of solar light/O_3 (flow rate = 1 L min^{-1}), 0.2 g of g-C_3N_4/Fe-MCM-48 catalyst showed 100% azithromycin (50 mg L^{-1}, 1 L) removal efficiency within 11 min (stable after fourth cycle). The pH (= 9) and Fe contents have influence on the degradation of azithromycin. In another study, ibuprofen was degraded by photocatalytic ozonation by using $SrWO_4$/ZnO composite (Alhumade et al., 2022). About 93% of 0.1 mg L^{-1} (300 mL) ibuprofen (BOD removal efficiency = 55%) was removed within 30 min by 0.35 g L^{-1} $SrWO_4$/(0.4%) ZnO composite under UV light illumination with ozone supply (using lab scale ozone generator). Lashuk et al. (2022) have used photocatalytic ozonation method to degrade per- and poly-fluoroalkyl substances in water by employing WO_3/TiO_2 composite as catalyst. Particularly, 5 wt%

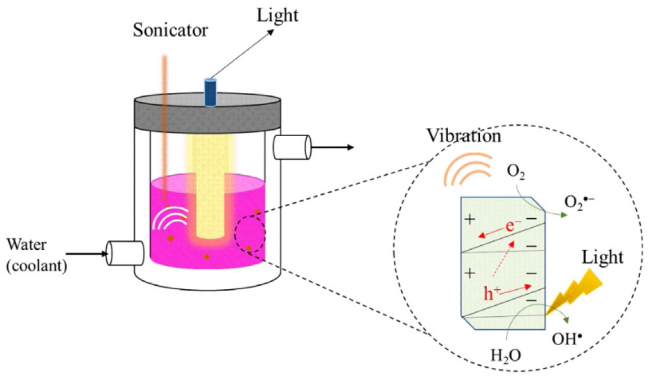

Fig. 5. Schematic representation of photo–piezocatalysis.

WO_3/TiO_2 showed the best photocatalytic property against methylene blue degradation. Also, degradation of per- and poly-fluoroalkyl substances is greater under UVA than UVA–visible light regions after 4 h. The removal of per- and poly-fluoroalkyl substances by this catalyst through photolysis and ozone photolysis is low, whereas photocatalytic ozonation exhibited high removal efficiency.

In literature, ternary composites were reported as catalysts in photo-ozonation technique. MnO_2-NH_2/graphene oxide/proton-functionalized g-C_3N_4 ternary nanocomposite was prepared and used for photocatalytic ozonation of cephalexin in water (Yang and Guan, 2022). Cephalexin degradation efficiency achieved via ozonation, catalytic ozonation is 20.3 (2 min) and 60.3% respectively. This composite catalyst produced hydroxyl radicals which is greater than catalytic ozonation and photocatalysis and thus cephalexin was removed within 2.5 min. The unique sandwich structure facilitates the electron transfer between proton-functionalized g-C_3N_4 and MnO_2-NH_2 via graphene oxide. It effectively hampers photoelectron–hole recombination and accelerates redox processes on MnO_2 ($Mn^{2+}/Mn^{3+}/Mn^{4+}$). Liu et al. (2022b) have prepared $Ag_2O/ZnO/g\text{-}C_3N_4$ composite through a precipitation-reflux approach and applied it as catalyst in the photocatalytic ozonation of (degradation) oxalic acid. About 83.43% of oxalic acid degradation efficiency ($k = 0.0311$ min^{-1}) was obtained for $Ag_2O/ZnO/g\text{-}C_3N_4$. It was due to the effective separation of photocharges, and the migration of electrons.

3.6. photo–piezocatalysis

Materials which produce an electric field (positive and negative charges) under an applied mechanical force (like vibration) are called piezoelectric materials. Piezoelectric materials transmute an electrical energy into mechanical energy or vice versa. Such materials are applied to expedite the degradation (piezocatalysis) of organic contaminants in polluted water. Piezo-materials such as hydroxyapatite ($Ca_{10}(PO_4)_6(OH)_2$), and sodium bismuth titanate ($Na_{0.5}Bi_{0.5}TiO_3$) has showed piezocatalytic properties (Shi et al., 2022a; Yin et al., 2023). Fig. 5 presented a schematic representation of photo–piezocatalysis.

The combination of semiconductor photocatalysts with piezoelectric properties could be useful to improve charge separation and migration and facilitate redox reactions. Photo–piezoelectric materials harvest light and mechanical energy and clean the wastewater. Generally, photo–piezocatalytic experiments are conducted in a photocatalytic reactor. The catalyst is dispersed in the aqueous solution of pollutants and stirred for a certain time period (usually 30 min) in the dark to attain absorption–desorption equilibrium. Then, the suspension is irradiated with ultrasonic vibration along with light (Shi et al., 2022a).

Nanocomposites with piezo behaviour have been applied as catalysts in photo–piezocatalytic degradation of pollutants. Dursun et al. (2021) have prepared lead magnesium niobate-lead titanate ($0.65Pb(Mg_{1/3}Nb_{2/3})O_3\text{-}0.35PbTiO_3$)/tin dioxide ($SnO_2$) heterostructure for the elimination of methylene blue under (250 W Metal halide lamp) visible light irradiation and ultrasonic wave vibrations (200 W, 45 kHz). At pH = 10, the heterostructured catalyst displayed complete methylene blue photodegradation within 120 min. Whereas, about 50 mg of the 1.75 wt% $0.65Pb(Mg_{1/3}Nb_{2/3})O_3\text{-}0.35PbTiO_3)/SnO_2$ catalyst can eliminate 100% of 20 mg L^{-1} (100 mL) methylene blue in water within 70 min. Wu et al. (2023) have constructed a ternary composite using ZIF-67N (sintered under nitrogen atmosphere), $BiFeO_3$ and CdS nanoparticles and used for degradation of bisphenol A under visible and near-infrared light ($\lambda \geq 700$ nm) and ultrasonic vibration. This ternary composite did not show significant degradation efficiency under ultrasound or light irradiation. But, under 40 kHz ultrasound and visible-light irradiations, this catalyst degraded ~85% bisphenol A within 160 min. At 68 kHz/visible light illumination, 91.2% of bisphenol A degradation efficiency was reported.

Composites containing plasmonic nanomaterials could show enhanced degradation activities. For instance, Shi et al. (2022b) have reported that the $Na_{0.5}Bi_{0.5}TiO_3$/Ag nanocomposite exhibits good rhodamine B degradation activity under piezo-photocatalytic experimental conditions (300 W Xe lamp illumination, ultrasound: 300 W, 40 kHz). About 98.8%

rhodamine B (5 mg L^{-1}, 20 mL) with the corresponding rate constant of $k = 0.146$ $min^{-1}$was eliminated within 30 min (highly stable after fifth cycle). Both Schottky junction surface plasmon resonance effects of Ag nanoparticles are the key reasons for great photocatalytic activity of $Na_{0.5}Bi_{0.5}TiO_3$/Ag composite. Li et al. (2022c) have prepared Au/$AgNbO_3$ nanocomposite (catalyst dosage = 50 mg) with significant rhodamine B (10 mg L^{-1}, 100 mL) degradation efficiency ($k = 0.054$ min^{-1}) under light (Xe lamp) irradiation and ultrasonic vibration (110 W, 40 kHz). The optimized catalyst (3 mL of $HAuCl_4 \bullet 3H_2O$ aqueous solution + 0.4 g $AgNbO_3$) showed complete removal of rhodamine B within 1 h. High photocatalytic performance of Au/$AgNbO_3$ is attributed to the surface plasmon resonance and piezotronics effect.

4. Photocatalysis integrated with multiple techniques

In spite of two integrated techniques, research has also been performed on integration of three techniques for effective removal of pollutants from water. Few recent studies are discussed below. Adsorption integrated photo-Fenton technique was developed for removal of fluoroquinolones (Gao et al., 2022). A poly(vinyl formal) sponge consisting of $MoS_2/Bi_2S_3/BiVO_4$/lignosulfonate was used in this integrated technique. The surface area and density of composite modified sponge is 9.025 m^2 g^{-1} and 0.134 g cm^{-3} respectively. About 92.8% norfloxacin removal efficiency was observed when contact time and pH is 60 min and 6.0 respectively. Adsorption efficiency of sponge and Mo(IV)/(VI) and Bi(III)/(V) redox couples promoted the degradation efficiency of the sponge catalyst. Polyvinyl alcohol (PVA) coated TiO_2/reduced graphene oxide/polyvinylidene fluoride (PVDF) photocatalytic membrane was used for treatment of Batik (textile industrial) wastewater through adsorption-ozonation-photocatalytic technique (Kusworo et al., 2022). TiO_2/rGO nanocomposite exhibits high visible light absorption (band gap = 2.9 eV), whereas PVA improved hydrophilicity of the modified membrane (pore radius = 2.77 ± 0.30 nm). This integrated adsorption-ozonation-photocatalytic filtration technology showed enhanced stability, and pollutant removal efficiency. Barium titanate ($BaTiO_3$)/TiO_2 composite was applied as a piezo-photoelectric catalyst in the degradation of indigo carmine (Liu et al., 2022c). $BaTiO_3/TiO_2$ (band gap = 2.89 eV) displays indigo carmine (10 mg L^{-1}, 100 mL) degradation rate constant of 0.109 min^{-1}. The 300 W Xenon lamp and 200 W ultrasonicator were used as light and mechanical strain sources, respectively. Both light illumination and ultrasonication generated electron–hole pairs which produce active free radicals for an effective degradation of indigo carmine in water. An integrated photocatalysis-ozonation-electrocatalytic technique was constructed for degradation of perfluorooctanoic acid (Li et al., 2020b). RGO/BiOCl nanocomposites were employed as catalysts. Perfluorooctanoic acid removal efficiency and degradation time was 95.4% and 3 h respectively. Only photocatalytic ozonation and photoelectro-peroxone processes showed removal efficiency of 80.5 and 56.1%, respectively. Both photoinduced hole (photocatalysis) and hydroxyl radical (electrocatalysis) played a role in the degradation of perfluorooctanoic acid.

5. Present challenges and future perspectives

Integrated photocatalytic technologies, utilizing nanocomposites are a rising research field. Nevertheless, these technologies have certain limitations which are highlighted below.
(a) Design and preparation of nanocomposites are essential to have high performances in integrated photocatalytic technologies.
(b) The environmental negative consequences of nanocomposites must be studied.
(c) Cost effective and eco-friendly nanocomposite photocatalysts should be explored. Scalable, cost effective and efficient catalysts need to be tested in integrated techniques.
(d) Theoretical simulations for prediction of catalytic ability of nanocomposites which are applying in integrated photocatalytic technologies are needed.
(e) There are limited studies in piezophotocatalytic technology.
(f) Solar-driven catalysts should be checked in integrated photocatalytic technologies.
(g) Nanocomposites containing toxic heavy metals should be avoided.
(h) Cost analysis and energy consumption of the integrated photocatalytic technologies need to be done.

6. Concluding remark and prospective views

The development of photocatalytic technology for degradation of chemical pollutants in water is significant. Different nanocomposite photocatalysts were fabricated for decomposition of specific water pollutants. For further improvement, photocatalysis was integrated with other water treatment methods. The synergistic effect between photocatalysis and adsorption, Fenton process, sonocatalysis, electrocatalysis, ozonation, piezocatalysis favours the efficient generation of free radicals (due to improved charge separation) which increased the pollutant removal performance of the nanocomposites. Nanocomposites composed of metal compounds, metals, carbon materials and polymers were extensively studied as catalysts in integrated photocatalytic techniques. The production of active species is dependent on the nanocomposite and the integrated system. Hydroxyl radicals, holes and superoxide anion radicals played a vital role in the degradation process. In adsorptive photocatalysis, the adsorbent component improves the adsorption as well as separation of charge carriers (like graphene). In photocatalytic ozonation, ozone produces active species via integrating with photocatalysis.

Both light and ultrasound waves (sonophotocatalysis) produce a huge number of active species through the nanocomposite catalysts. Iron-based nanocomposites generate huge concentrations of hydroxyl radicals by photo-Fenton process. External bias voltage effectively separates photo-generated charges, thereby achieving enhanced degradation efficiency. The degradation performance of nanocomposites depends on initial pH, dosage, initial concentration of pollutants and molecular structure of the pollutants. This review emphasized the development of integrated photocatalytic technology for wastewater treatment application. Besides the development, integrated photocatalytic techniques required more studies using various pollutants and new catalysts.

CRediT authorship contribution statement

R. Suresh: Conceptualization, Methodology, Data curation, Writing – original draft. **Lalitha Gnanasekaran:** Writing – review & editing, Validation. **Saravanan Rajendran:** Conceptualization, Resources, Visualization, Project administration, Supervision, Funding acquisition, Writing – original draft, Writing – review & editing, Validation. **Matias Soto-Moscoso:** Writing – review & editing, Validation. **Wei-Hsin Chen:** Writing – review & editing, Validation. **Pau Loke Show:** Writing – review & editing, Validation. **Kuan Shiong Khoo:** Writing – review & editing, Supervision, Validation.

Declaration of competing interest

The authors declare that they have no known competing financial interests or personal relationships that could have appeared to influence the work reported in this paper.

Acknowledgement

The author (SR) acknowledges the support of ANID, Chile through the project FONDECYT REGULAR No: 1220663.

References

Abazari, R., Mahjoub, A.R., Sanati, S., Rezvani, Z., Hou, Z., Dai, H., 2019. Ni-Ti layered double hydroxide@graphitic carbon nitride nanosheet: A novel nanocomposite with high and ultrafast sonophotocatalytic performance for degradation of antibiotics. Inorg. Chem. 58, 1834–1849. http://dx.doi.org/10.1021/acs.inorgchem.8b02575.

Abbasi, M.Ali., Amin, K.M., Ali, M., Ali, Z., Atif, M., Ensinger, W., Khalid, W., 2022. Synergetic effect of adsorption-photocatalysis by GO - CeO_2 nanocomposites for photodegradation of doxorubicin. J. Environ. Chem. Eng. 10, 107078. http://dx.doi.org/10.1016/j.jece.2021.107078.

Al-Musawi, T.J., Mengelizadeh, N., Kassim, W.M.S., Sillanpaa, M., Siddiqui, S.H., Shahbaksh, S., Balarak, D., 2022. Sonophotocatalytic degradation and operational parameters optimization of diazinon using magnetic cobalt–graphene nanocomposite as a catalyst. J. Water Process. Eng 46, 102548. http://dx.doi.org/10.1016/j.jwpe.2021.102548.

Alhumade, H., Akhtar, J., Al-Shahrani, S., Moujdin, I.A., Tahir, M.B., 2022. Ozonation of ibuprofen in presence of $SrWO_4$/ZnO photo-catalyst. Emerg. Contam. 8, 391–399. http://dx.doi.org/10.1016/j.emcon.2022.10.001.

Bayan, E.M., Pustovaya, L.E., Volkova, M.G., 2021. Recent advances in TiO_2-based materials for photocatalytic degradation of antibiotics in aqueous systems. Environ. Technol. Innov. 24, 101822. http://dx.doi.org/10.1016/j.eti.2021.101822.

Chandrabose, G., Dey, A., Gaur, S.S., Pitchaimuthu, S., Jagadeesan, H., Braithwaite, N.S.J., Selvaraj, V., Kumar, V., Krishnamurthy, S., 2021. Removal and degradation of mixed dye pollutants by integrated adsorption-photocatalysis technique using 2-D MoS_2/TiO_2 nanocomposite. Chemosphere 279, 130467. http://dx.doi.org/10.1016/j.chemosphere.2021.130467.

Chen, X., Chen, J., Li, N., Li, J., He, J., Xu, S., Zhu, Y., Yao, L., Lai, Y., Zhu, R., 2023c. Ag_3PO_4-anchored $La_2Ti_2O_7$ nanorod as a Z-scheme heterostructure composite with boosted photogenerated carrier separation and enhanced photocatalytic performance under natural sunlight. Environ. Pollut. 323, 121322. http://dx.doi.org/10.1016/j.envpol.2023.121322.

Chen, R., Ding, S., Fu, N., Ren, X., 2023b. Preparation of a g-C_3N_4/Ag_3PO_4 composite Z-type photocatalyst and photocatalytic degradation of ofloxacin: Degradation performance, reaction mechanism, degradation pathway and toxicity evaluation. J. Environ. Chem. Eng. 11, 109440. http://dx.doi.org/10.1016/j.jece.2023.109440.

Chen, X., Wu, R., Wu, H., Hu, Y., Wang, H., Fu, J., Pi, J., Xu, Y., 2023a. Integrated miRNA-mRNA analysis reveals the dysregulation of lipid metabolism in mouse liver induced by developmental arsenic exposure. J. Hazard. Mater 445, 130459. http://dx.doi.org/10.1016/j.jhazmat.2022.130459.

Cuprys, A., Pulicharla, R., Lecka, J., Brar, S.K., Drogui, P., Surampalli, R.Y., 2018. Ciprofloxacin-metal complexes estability and toxicity tests in the presence of humic substances. Chemosphere 202, 549–559. http://dx.doi.org/10.1016/j.chemosphere.2018.03.117.

De, I., Pahuja, M., Wani, H.Mohi.ud.din., Dey, A., Dube, T., Ghosh, R., Kankan, N., Mishra, J., Panda, J.J., Maruyama, T., Ghosh, K., Singh, M., 2022. In-vitro toxicity assessment of a textile dye eriochrome black T and its nano-photocatalytic degradation through an innovative approach using Mf-NGr-CNTs-SnO_2 heterostructures. Ecotoxicol. Environ. Saf. 243, 113985. http://dx.doi.org/10.1016/j.ecoenv.2022.113985.

Dileep Kumar, V.G., Kumari, S., Balaji, K.R., Khan, A.A., Ravikumar, C.R., Basavaraja, B.M., Santosh, M.S., Rtimi, S., 2023. Singlet oxygen driven enhanced photocatalytic degradation of 1, 3, 7-trimethylpurine-2, 6-Dione using surfactant mediated PVA-CuO nanocomposites: Combining physical adsorption and photocatalysis. Chem. Eng. J. 462, 142187. http://dx.doi.org/10.1016/j.cej.2023.142187.

Ding, Z., Sun, M., Liu, W., Sun, W., Meng, X., Zheng, Y., 2021. Ultrasonically synthesized N-TiO_2/Ti_3C_2 composites: Enhancing sonophotocatalytic activity for pollutant degradation and nitrogen fixation. Sep. Purif. Technol. 276, 119287. http://dx.doi.org/10.1016/j.seppur.2021.119287.

Ding, H., Zahid, A.H., Han, Q., 2023. Synthesis of 3D flowerlike S-scheme $Bi_4O_5I_2$/BiOI heterojunction with synergistic effect of adsorption and photocatalysis. Mater. Sci. Eng. B 289, 116209. http://dx.doi.org/10.1016/j.mseb.2022.116209.

Du, B., Fan, G., Yang, S., Chen, Z., Luo, J., Yu, W., Yu, J., Wei, Q., Lu, Y., 2022. Sonophotocatalytic degradation of 17β-estradiol by Er^{3+}-CdS/MoS_2: The role and transformation of reactive oxygen species. J. Clean. Prod. 333, 130203. http://dx.doi.org/10.1016/j.jclepro.2021.130203.

Dursun, S., Akyildiz, H., Kalem, V., 2021. PMN-PT nanoparticle/SnO_2 nanofiber heterostructures: Enhanced photocatalytic degradation performance by ultrasonic wave induced piezoelectric field. J. Alloys Compd. 889, 161769. http://dx.doi.org/10.1016/j.jallcom.2021.161769.

Fan, G., Yang, S., Du, B., Luo, J., Lin, X., Li, X., 2022. Sono-photo hybrid process for the synergistic degradation of levofloxacin by $FeVO_4$/$BiVO_4$: Mechanisms and kinetics. Environ. Res. 204, 112032. http://dx.doi.org/10.1016/j.envres.2021.112032.

Feng, D., He, J., Zheng, L., Jiang, W., Zhang, C., Li, L., Song, J., Yao, W., 2021. Enhanced catalytic performance with Fe@α-Fe_2O_3 thin nanosheets by synergistic effect of photocatalysis and fenton-like process. J. Phys. Chem. Solids 150, 109886. http://dx.doi.org/10.1016/j.jpcs.2020.109886.

Gao, B., Pan, Y., Yang, H., 2022. Enhanced photo-Fenton degradation of fluoroquinolones in water assisted by a 3D composite sponge complexed with a S-scheme $MoS_2/Bi_2S_3/BiVO_4$ ternary photocatalyst. Appl. Catal. 315, 121580. http://dx.doi.org/10.1016/j.apcatb.2022.121580.

Guo, F., Huang, X., Chen, Z., Cao, L., Cheng, X., Chen, L., Shi, W., 2021. Construction of Cu_3P-$ZnSnO_3$-g-C_3N_4 p-n-n heterojunction with multiple built-in electric fields for effectively boosting visible-light photocatalytic degradation of broad-spectrum antibiotics. Sep. Purif. Technol. 265, 118477. http://dx.doi.org/10.1016/j.seppur.2021.118477.

Guo, B., Liu, B., Wang, C., Wang, Y., Yin, S., Javed, M.S., Han, W., 2022. S-scheme $Ti_{0.7}Sn_{0.3}O_2$/g-C_3N_4 heterojunction composite for enhanced photocatalytic pollutants degradation. J. Environ. Chem. Eng. 10, 107118. http://dx.doi.org/10.1016/j.jece.2021.107118.

Hayati, F., Khodabakhshi, M.R., Isari, A.A., Moradi, S., Kakavandi, B., 2020. LED-assisted sonocatalysis of sulfathiazole and pharmaceutical wastewater using N, Fe Co-doped TiO_2@SWCNT: Optimization, performance and reaction mechanism studies. J. Water Process. Eng. 38, 101693. http://dx.doi.org/10.1016/j.jwpe.2020.101693.

Henriques, B., Rodrigues, S.M., Coelho, C., Cruz, N., Duarte, A.C., Römkens, P.F.A.M., Pereira, E., 2013. Risks associated with the transfer of toxic organo-metallic mercury from soils into the terrestrial feed chain. Environ. Int. 59, 408–417. http://dx.doi.org/10.1016/j.envint.2013.07.006.

Hu, Z., Ge, M., Guo, C., 2021. Efficient removal of levofloxacin from different water matrices via simultaneous adsorption and photocatalysis using a magnetic Ag_3PO_4/rGO/$CoFe_2O_4$ catalyst. Chemosphere 268, 128834. http://dx.doi.org/10.1016/j.chemosphere.2020.128834.

Hu, J., Li, J., Cui, J., An, W., Liu, L., Liang, Y., Cui, W., 2020a. Surface oxygen vacancies enriched FeOOH/Bi_2MoO_6 photocatalysis- Fenton synergy degradation of organic pollutants. J. Hazard. Mater. 384, 121399. http://dx.doi.org/10.1016/j.jhazmat.2019.121399.

Hu, J., Zhang, P., Cui, J., An, W., Liu, L., Liang, Y., Yang, Q., Yang, H., Cui, W., 2020b. High-efficiency removal of phenol and coking wastewater via photocatalysis-Fenton synergy over a Fe-g-C_3N_4 graphene hydrogel 3D structure. J. Ind. Eng. Chem. 84, 305–314. http://dx.doi.org/10.1016/j.jiec.2020.01.012.

Huang, X., Zhou, H., Yue, X., Ran, S., Zhu, J., 2021. Novel magnetic Fe_3O_4/α-FeOOH nanocomposites and their enhanced mechanism for tetracycline hydrochloride removal in the visible photo-Fenton process. ACS Omega 6, 9095–9103. http://dx.doi.org/10.1021/acsomega.1c00204.

Jakobczyk-Karpierz, S., Slosarczyk, K., 2022. Isotopic signature of anthropogenic sources of groundwater contamination with sulfate and its application to groundwater in a heavily urbanized and industrialized area (Upper Silesia, Poland). J. Hydrol 612, 128255. http://dx.doi.org/10.1016/j.jhydrol.2022.128255.

Ji, Z., Yang, X., Qi, X., Zhang, H., Zhang, Y., Xia, X., Pei, Y., 2022. Facile synthesis of waste-based CdS-loaded hierarchically porous geopolymer for adsorption-photocatalysis of organic contamination and its environmental risks. Chemosphere 308, 136144. http://dx.doi.org/10.1016/j.chemosphere.2022.136144.

Jiang, S., Zheng, H., Sun, X., Zhu, M., Zhou, Y., Wang, D., Zhang, D., Zhang, L., 2022. New and highly efficient ultra-thin g-C_3N_4/FeOCl nanocomposites as photo-Fenton catalysts for pollutants degradation and antibacterial effect under visible light. Chemosphere 290, 133324. http://dx.doi.org/10.1016/j.chemosphere.2021.133324.

Ju, L., Wu, P., Ju, Y., Chen, M., Yang, S., Zhu, H., 2021. The degradation mechanism of Bisphenol A by photoelectrocatalysis using new materials as the working electrode. Surf. Interfaces 23, 100967. http://dx.doi.org/10.1016/j.surfin.2021.100967.

Kakavandi, B., Bahari, N., Kalantary, R.R., Fard, E.D., 2019. Enhanced sono-photocatalysis of tetracycline antibiotic using TiO_2 decorated on magnetic activated carbon (MAC@T) coupled with US and UV: A new hybrid system. Ultrason. Sonochem. 55, 75–85. http://dx.doi.org/10.1016/j.ultsonch.2019.02.026.

Karjalainen, J., Makinen, M., Karjalainen, A.K., 2021. Sulfate toxicity to early life stages of European whitefish (*Coregonus lavaretus*) in soft freshwater. Ecotoxicol. Environ. Saf. 208, 111763. http://dx.doi.org/10.1016/j.ecoenv.2020.111763.

Kaur, P., Park, Y., Sillanpaa, M., Imteaz, M.A., 2021. Synthesis of a novel SnO_2/graphene-like carbon/TiO_2 electrodes for the degradation of recalcitrant emergent pharmaceutical pollutants in a photo-electrocatalytic system. J. Clean. Prod. 313, 127915. http://dx.doi.org/10.1016/j.jclepro.2021.127915.

Khairy, M., Naguib, E.M., Mohamed, M.M., 2020. Enhancement of photocatalytic and sonophotocatalytic degradation of 4-nitrophenol by ZnO/graphene oxide and ZnO/carbon nanotube nanocomposites. J. Photochem. Photobiol. A: Chem 396, 112507. http://dx.doi.org/10.1016/j.jphotochem.2020.112507.

Khan, M.F., Cazzato, G., Saleemi, H.A., Macadangdang, R.R., Aftab, M.N., Ismail, M., Khalid, H., Ali, S., Bakhtiar, S.U.H., Ismail, A., Zahid, M., 2022. Sonophotocatalytic degradation of organic pollutant under visible light over Pt decorated CeO_2: Role of ultrasonic waves for unprecedented degradation. J. Mol. Struct. 1247, 131397. http://dx.doi.org/10.1016/j.molstruc.2021.131397.

Köktürk, M., 2022. In vivo toxicity assessment of Remazol Gelb–GR (RG-GR) textile dye in zebrafish embryos/larvae (danio rerio): Teratogenic effects, biochemical changes, immunohistochemical changes. Sci. Total Environ. 852, 158473. http://dx.doi.org/10.1016/j.scitotenv.2022.158473.

Krishnan, R.Y., Manikandan, S., Subbaiya, R., Biruntha, M., Govarthanan, M., Karmegam, N., 2021. Removal of emerging micropollutants originating from pharmaceuticals and personal care products (PPCPs) in water and wastewater by advanced oxidation processes: A review. Environ. Technol. Innov. 23, 101757. http://dx.doi.org/10.1016/j.eti.2021.101757.

Kuang, X., Fu, M., Kang, H., Lu, P., Bai, J., Yang, Y., Gao, S., 2023. A $BiOIO_3$/BiOBr n-n heterojunction was constructed to enhance the photocatalytic degradation of TC. Opt. Mater. 138, 113690. http://dx.doi.org/10.1016/j.optmat.2023.113690.

Kumar, V., Sharma, H., Chaudhary, V., Yadav, M.K., Singh, V.N., Surbhi, 2022. Ag coated CuS core/shell nanoparticles to harness the full vis-NIR spectrum for photocatalysis. Chem. Phys. Lett. 807, 140117. http://dx.doi.org/10.1016/j.cplett.2022.140117.

Kusworo, T.D., Irvan, A.C., Nabilah, Y., Rasendriya, A., Utomo, D.P., Hasbullah, H., 2022. Advanced method for clean water recovery from batik wastewater via sequential adsorption, ozonation and photocatalytic membrane PVDF-TiO_2/RGO processes. J. Environ. Chem. Eng. 10, 108708. http://dx.doi.org/10.1016/j.jece.2022.108708.

Lashuk, B., Pineda, M., AbuBakr, S., Boffito, D., Yargeau, V., 2022. Application of photocatalytic ozonation with a WO_3/TiO_2 catalyst for PFAS removal under UVA/visible light. Sci. Total Environ. 843, 157006. http://dx.doi.org/10.1016/j.scitotenv.2022.157006.

Lenz, M.E., PAS, J.K., Kern, R.J., Orvis, C.E., Drewnoski, M.E., 2019. Nitrate toxicity in annual forages: Survey of beef producer perspectives and samples submitted to a commercial testing laboratory in Nebraska. Applied Animal Science 35, 455–463. http://dx.doi.org/10.15232/aas.2019-01865.

Li, J., Ding, Y., Chen, K., Li, Z., Yang, H., Yue, S., Tang, Y., Wang, Q., 2022b. δ-FeOOH coupled BiOBr $_{0.5}I_{0.5}$ for efficient photocatalysis-Fenton synergistic degradation of organic pollutants. J. Alloys Compd. 903, 163795. http://dx.doi.org/10.1016/j.jallcom.2022.163795.

Li, R., Hu, X., Yu, Y., Xu, W., Chen, D., Zhu, X., Tang, Y., Yao, L., Qin, J., Fang, J., Liu, Z., Fang, Z., 2022a. Anatase quantum dots decorated silica/carbon lamellas for removal of antipsychotic drugs via adsorption-photocatalysis and toxicity evaluation. Chemosphere 303, 134972. http://dx.doi.org/10.1016/j.chemosphere.2022.134972.

Li, Z., Li, S., Tang, Y., Li, X., Wang, J., Li, L., 2020b. Highly efficient degradation of perfluorooctanoic acid: An integrated photoelectrocatalytic ozonation and mechanism study. Chem. Eng. J. 391, 123533. http://dx.doi.org/10.1016/j.cej.2019.123533.

Li, T., Liang, J., Zhou, L., 2020a. Fabricating Fe_3O_4-Schwertmannite as a Z-scheme photocatalyst with excellent photocatalysis-Fenton reaction and recyclability. J. Environ. Sci 98, 186–195. http://dx.doi.org/10.1016/j.jes.2020.06.005.

Li, X., Lu, S., Zhang, G., 2023b. Three-dimensional structured electrode for electrocatalytic organic wastewater purification: Design, mechanism and role. J. Hazard. Mater 445, 130524. http://dx.doi.org/10.1016/j.jhazmat.2022.130524.

Li, Y., Sun, X., Tang, Y., Ng, Y.H., Li, L., Jiang, F., Wang, J., Chen, W., Li, L., 2021a. Understanding photoelectrocatalytic degradation of tetracycline over three-dimensional coral-like ZnO/$BiVO_4$ nanocomposite. Mater. Chem. Phys. 271, 124871. http://dx.doi.org/10.1016/j.matchemphys.2021.124871.
Li, C., Tan, X., Ma, J., 2021b. Concerted high innergenerated-H_2O_2 photocatalysis and photo-Fenton degradation of organic pollutants over SCNO@CdS. J. Photochem. Photobiol. A: Chem 420, 113477. http://dx.doi.org/10.1016/j.jphotochem.2021.113477.
Li, J.J., Yue, Y.X., Jiang, J.F., Shi, S.J., Wu, H.X., Zhao, Y.H., Che, F.F., 2023a. Assessment of toxic mechanisms and mode of action to three different levels of species for 14 antibiotics based on interspecies correlation, excess toxicity, and QSAR. Chemosphere 317, 137795. http://dx.doi.org/10.1016/j.chemosphere.2023.137795.
Li, S., Zhao, Z., Liu, M., Liu, X., Huang, W., Sun, S., Jiang, Y., Liu, Y., Zhang, J., Zhang, Z., 2022c. Remarkably enhanced photocatalytic performance of Au/$AgNbO_3$ heterostructures by coupling piezotronic with plasmonic effects. Nano Energy 95, 107031. http://dx.doi.org/10.1016/j.nanoen.2022.107031.
Lin, Y.H., Tseng, W.J., 2022. Multifunctional Fe_3O_4@Ag@$TiO_{2-x}N_x$ core-shell composite particles for dye adsorption and visible-light photocatalysis. Ceram. Int. 48, 13906–13913. http://dx.doi.org/10.1016/j.ceramint.2022.01.275.
Ling, Y., Liu, H., Li, B., Zhang, B., Wu, Y., Hu, H., Yu, D., Huang, S., 2023. Efficient photocatalytic ozonation of azithromycin by three-dimensional g-C_3N_4 nanosheet loaded magnetic Fe-MCM-48 under simulated solar light. Appl. Catal. 324, 122208. http://dx.doi.org/10.1016/j.apcatb.2022.122208.
Liu, Q., Hou, J., Zeng, Y., Xia, J., Miao, L., Wu, J., 2023. Integrated photocatalysis and moving bed biofilm reactor (MBBR) for treating conventional and emerging organic pollutants from synthetic wastewater: Performances and microbial community responses. Bioresour. Technol. 370, 128530. http://dx.doi.org/10.1016/j.biortech.2022.128530.
Liu, Q., Li, Z., Li, J., Zhan, F., Zhai, D., Sun, Q., Xiao, Z., Luo, H., Zhang, D., 2022c. Three dimensional $BaTiO_3$ piezoelectric ceramics coated with TiO_2 nanoarray for high performance of piezo-photoelectric catalysis. Nano Energy 98, 107267. http://dx.doi.org/10.1016/j.nanoen.2022.107267.
Liu, J., Shi, H., Sans, C., Sun, L., Yuan, X., Pan, F., Xia, D., 2022b. Insights into the photocatalytic ozonation over Ag_2O-ZnO@g-C_3N_4 composite: Cooperative structure, degradation performance, and synergistic mechanisms. J. Environ. Chem. Eng. 10, 107285. http://dx.doi.org/10.1016/j.jece.2022.107285.
Liu, T., Wang, Z., Wang, X., Yang, G., Liu, Y., 2021. Adsorption-photocatalysis performance of polyaniline/dicarboxyl acid cellulose@graphene oxide for dye removal. International J. Biol. Macromol. 182, 492–501. http://dx.doi.org/10.1016/j.ijbiomac.2021.04.038.
Liu, C., Zhu, C., Wang, H., Xie, S., Zhou, J., Fang, H., 2022a. Synergistic removal of organic pollutants by co-doped MIL-53(Al) composite through the integrated adsorption/photocatalysis. J. Solid State Chem. 316, 123582. http://dx.doi.org/10.1016/j.jssc.2022.123582.
Lu, S., Ma, Y., Zhao, L., 2022b. Production of ZnO-CoO_x-CeO_2 nanocomposites and their dye removal performance from wastewater by adsorption-photocatalysis. J. Mol. Liq 364, 119924. http://dx.doi.org/10.1016/j.molliq.2022.119924.
Lu, Y., Zhang, H., Fan, D., Chen, Z., Yang, X., 2022a. Coupling solar-driven photothermal effect into photocatalysis for sustainable water treatment. J. Hazard. Mater. 423, 127128. http://dx.doi.org/10.1016/j.jhazmat.2021.127128.
Lucero Rincon, C.H., Pena Salamanca, E.J., Cantera Kintz, J.R., Lizcano, O.V., Cruz-Quintana, Y., Neira, R., 2023. Assessment of mercury and lead contamination using the bivalve *Anadara tuberculosa* (Arcidae) in an estuary of the Colombian Pacific. Mar. Pollut. Bull. 187, 114519. http://dx.doi.org/10.1016/j.marpolbul.2022.114519.
Luo, Y., Zheng, A., Li, J., Han, Y., Xue, M., Zhang, L., Yin, Z., Xie, C., Chen, Z., Ji, L., Hong, Z., Xie, X., 2023. Integrated adsorption and photodegradation of tetracycline by bismuth oxycarbonate/biochar nanocomposites. Chem. Eng. J. 457, 141228. http://dx.doi.org/10.1016/j.cej.2022.141228.
Ly, Q.V., Cui, L., Asif, M.B., Khan, W., Nghiem, L.D., Hwang, Y., Zhang, Z., 2023. Membrane-based nanoconfined heterogeneous catalysis for water purification: A critical review. Water Res. 230, 119577. http://dx.doi.org/10.1016/j.watres.2023.119577.
Ma, P., Yu, Y., Xie, J., Fu, Z., 2017. Ag_3PO_4/CuO composites utilizing the synergistic effect of photocatalysis and fenton-like catalysis to dispose organic pollutants. Adv. Powder Technol. 28, 2797–2804. http://dx.doi.org/10.1016/j.apt.2017.08.004.
Mahabeer, P., Tekere, M., 2021. Anthropogenic pollution influences on the physical and chemical quality of water and sediments of the umdloti river system. Kwazulu-Natal. Phys. Chem. Earth. 123, 103030. http://dx.doi.org/10.1016/j.pce.2021.103030.
Mao, W., Zhang, L., Zhang, Y., Wang, Y., Wen, N., Guan, Y., 2022. Adsorption and photocatalysis removal of arsenite, arsenate, and hexavalent chromium in water by the carbonized composite of manganese-crosslinked sodium alginate. Chemosphere 292, 133391. http://dx.doi.org/10.1016/j.chemosphere.2021.133391.
Marinho, B.A., Suhadolnik, L., Likozar, B., Hus, M., Marinko, ˇZ., ˇCeh, M., 2022. Photocatalytic, electrocatalytic and photoelectrocatalytic degradation of pharmaceuticals in aqueous media: Analytical methods, mechanisms, simulations, catalysts and reactors. J. Clean. Prod. 343, 131061. http://dx.doi.org/10.1016/j.jclepro.2022.131061.
Masekela, D., Mbita, N.C.H., Sam, S., Yusuf, T.L., Mabuba, N., 2023. Application of $BaTiO_3$-based catalysts for piezocatalytic, photocatalytic and piezophotocatalytic degradation of organic pollutants and bacterial disinfection in wastewater: A comprehensive review. Arab. J. Chem 16, 104473. http://dx.doi.org/10.1016/j.arabjc.2022.104473.
Maswanganyi, S., Gusain, R., Kumar, N., Fosso-Kankeu, E., Waanders, F.B., Ray, S.S., 2021. Bismuth molybdate nanoplates supported on reduced graphene oxide: An effective nanocomposite for the removal of naphthalene via adsorption-photodegradation. ACS Omega 6, 16783–16794. http://dx.doi.org/10.1021/acsomega.1c01296.
Mazarji, M., Esmaili, H., Bidhendi, G.N., Mahmoodi, N.M., Minkina, T., Sushkova, S., Mandzhieva, S., Barakhov, A., Moghtaderi, H., Bhatnagar, A., 2021. Green synthesis of reduced graphene oxide-$CoFe_2O_4$ nanocomposite as a highly efficient visible-light-driven catalyst in photocatalysis and photo fenton-like reaction. Mater. Sci. Eng. B 270, 115223. http://dx.doi.org/10.1016/j.mseb.2021.115223.
Moradeeya, P.G., Kumar, M.Anil., Sharma, A., Basha, S., 2022. Conductive polymer layered semiconductor for degradation of triclopyr acid and 2, 4-dichlorophenoxyacetic acid from aqueous stream using coalesce adsorption-photocatalysis technique. Chemosphere 298, 134360. http://dx.doi.org/10.1016/j.chemosphere.2022.134360.
Motlagh, P.Y., Akay, S., Kayan, B., Khataee, A., 2021. Ultrasonic assisted photocatalytic process for degradation of ciprofloxacin using TiO_2-Pd nanocomposite immobilized on pumice stone. Ind. Eng. Chem. Res 104, 582–591. http://dx.doi.org/10.1016/j.jiec.2021.09.007.
Ngigi, E.M., Nomngongo, P.N., Ngila, J.C., 2019. Novel Z-scheme Co_3O_4/WO_3 nanocomposite performance in adsorption and photocatalytic degradation of ethylparaben and methylene blue in water. Adv. Nat. Sci.: Nanosci. Nanotechnol. 10, 045018. http://dx.doi.org/10.1088/2043-6254/ab49f6, (12pp).
Nyankson, E., Efavi, J.K., Agyei-Tuffour, B., Manu, G., 2021. Synthesis of TiO_2–Ag_3PO_4 photocatalyst material with high adsorption capacity and photocatalytic activity: Application in the removal of dyes and pesticides. RSC Adv. 11, 17032–17045. http://dx.doi.org/10.1039/d1ra02128a.
Okpara, E.C., Olatunde, O.C., Wojuola, O.B., Onwudiwe, D.C., 2023. Applications of transition metal oxides and chalcogenides and their composites in water treatment: A review. Environ. Adv. 11, 100341. http://dx.doi.org/10.1016/j.envadv.2023.100341.
Peng, X., Tian, J., Zhang, S., Xiao, W., Tian, X., Wang, Y., Xue, J., Lei, D., 2023. Z-scheme transfer pathway assisted photoelectrocatalyst Zn_2SnO_4/rGO/Ag/AgBr for organic pollutants treatment. Colloids Surf. A Physicochem. Eng. Asp 657, 130552. http://dx.doi.org/10.1016/j.colsurfa.2022.130552.
Pervez, M. Nahid., Ma, S., Huang, S., Naddeo, V., Zhao, Y., 2022. Photo-Fenton degradation of ciprofloxacin by novel graphene quantum dots/α-FeOOH nanocomposites for the production of safe drinking water from surface water. Water 14 (2260), http://dx.doi.org/10.3390/w14142260.

Qing, Y., Li, Y., Guo, Z., Yang, Y., Li, W., 2022. Photocatalytic Bi_2WO_6/pg-C_3N_4-embedded in polyamide microfiltration membrane with enhanced performance in synergistic adsorption-photocatalysis of 17β-estradiol from water. J. Environ. Chem. Eng 10, 108648. http://dx.doi.org/10.1016/j.jece.2022.108648.

Rad, T.S., Khataee, A., Arefi-Oskoui, S., Rad, S.S., Orooji, Y., Gengec, E., Kobya, M., 2022b. Graphene-based ZnCr layered double hydroxide nanocomposites as bactericidal agents with high sonophotocatalytic performances for degradation of rifampicin. Chemosphere 286, 131740. http://dx.doi.org/10.1016/j.chemosphere.2021.131740.

Rad, T.S., Khataee, A., Rad, S.S., Arefi-Oskoui, S., Gengec, E., Kobya, M., Yoon, Y., 2022a. Zinc-chromium layered double hydroxides anchored on carbon nanotube and biochar for ultrasound-assisted photocatalysis of rifampicin. Ultrason. Sonochem 82, 105875. http://dx.doi.org/10.1016/j.ultsonch.2021.105875.

Rad, T.S., Yazici, E.S., Khataee, A., Gengec, E., Kobya, M., 2023. Ultrasound-assisted photocatalytic decomposition of rifadin with biochar and CNT-based NiCr layered double hydroxides. Surf. Interfaces 36, 102628. http://dx.doi.org/10.1016/j.surfin.2022.102628.

Rajendran, S., Hoang, T.K.A., Trudeau, M.L., Jalil, A.A., Naushad, M., Awual, M.R., 2022. Generation of novel n-p-n (CeO_2-PPy-ZnO) heterojunction for photocatalytic degradation of micro-organic pollutants. Environ. Pollut. 292, 118375. http://dx.doi.org/10.1016/j.envpol.2021.118375.

Rani, M., Yadav, J., Shanker, U., Sillanpaa, M., 2023. Green synthesized zinc derived nanocomposites with enhanced photocatalytic activity: An updated review on structural modification, scientific assessment and environmental applications. Inorg. Chem. Commun. 147, 110246. http://dx.doi.org/10.1016/j.inoche.2022.110246.

Ren, J., Meng, Y., Zhang, X., Gao, Y., Liu, L., Zhou, X., Zhang, Z., Zeng, L., Ke, J., 2022. Self-assembled perylene diimide modified NH_2-UiO-66 (Zr) construct n-n heterojunction catalysts for enhanced Cr(VI) photocatalytic reduction. Sep. Purif. Technol. 296, 121423. http://dx.doi.org/10.1016/j.seppur.2022.121423.

Riaz, R., Ali, M., Anwer, H., Ko, M.J., Jeong, S.H., 2019. Highly porous self-assembly of nitrogen-doped graphene quantum dots over reduced graphene sheets for photo-electrocatalytic electrode. J. Colloid Interface Sci. 557, 174–184. http://dx.doi.org/10.1016/j.jcis.2019.09.028.

Sabzehmeidani, M.M., Karimi, H., Ghaedi, M., 2020. Ceo_2 nanofibers-cds nanostructures n–n junction with enhanced visible-light photocatalytic activity. Arab. J. Chem. 13, 7583–7597. http://dx.doi.org/10.1016/j.arabjc.2020.08.015.

Saian, G., Gopalan, A.I., Wang, L., Venkatramanan, K., Roy, V.A.L., Sonar, P., Lee, D.E., Naidu, R., 2022. Conducting polymer based visible light photocatalytic composites for pollutant removal: Progress and prospects. Environ. Technol. Innov. 28, 102698. http://dx.doi.org/10.1016/j.eti.2022.102698.

Saleh, I.A., Zouari, N., Al-Ghouti, M.A., 2020. Removal of pesticides from water and wastewater: Chemical, physical and biological treatment approaches. Environ. Technol. Innov. 19, 101026. http://dx.doi.org/10.1016/j.eti.2020.101026.

Santana, R.M.D.R., Napoleao, D.C., Rodriguez-Diaz, J.M., Gomes, R.K.D.M., Silva, M.G., Garcia, R.R.P., Vinhas, G.M., Duarte, M.M.M.B., 2023. Original nanostructured bacterial cellulose/pyrite composite: Photocatalytic application in advanced oxidation processes. Chemosphere 319, 137953. http://dx.doi.org/10.1016/j.chemosphere.2023.137953.

Saravanan, A., Deivayanai, V.C., Senthil Kumar, P., Rangasamy, G., Hemavathy, R.V., Harshana, T., Gayathri, N., Alagumalai, K., 2022. A detailed review on advanced oxidation process in treatment of wastewater: Mechanism, challenges and future outlook. Chemosphere 308, 136524. http://dx.doi.org/10.1016/j.chemosphere.2022.136524.

Shakeel, M., Arif, M., Yasin, G., Li, B., Khan, H.D., 2019. Layered by layered Ni-Mn-LDH/g-C_3N_4 nanohybrid for multi-purpose photo/electrocatalysis: Morphology controlled strategy for effective charge carriers separation. Appl. Catal. B 242, 485–498. http://dx.doi.org/10.1016/j.apcatb.2018.10.005.

Shi, L., Lu, C., Chen, L., Zhang, Q., Li, Y., Zhang, T., Hao, X., 2022a. Piezocatalytic performance of $Na_{0.5}Bi_{0.5}TiO_3$ nanoparticles for degradation of organic pollutants. J. Alloys Compd. 895, 162591. http://dx.doi.org/10.1016/j.jallcom.2021.162591.

Shi, J., Xie, Z., Tang, X., Wang, Y., Yuan, G., Liu, J.M., 2022b. Enhanced piezo-photocatalytic performance of Ag@$Na_{0.5}Bi_{0.5}TiO_3$ composites. J. Alloys Compd. 911, 164885. http://dx.doi.org/10.1016/j.jallcom.2022.164885.

Sodeinde, K.O., Olusanya, S.O., O.S., Lawal., M., Sriariyanun., A.A., Adediran., 2022. Enhanced adsorptional-photocatalytic degradation of chloramphenicol by reduced graphene oxide-zinc oxide nanocomposite. Sci. Rep. 12, 17054. http://dx.doi.org/10.1038/s41598-022-21266-5.

Song, C., Chen, K., Chen, M., Jin, X., Liu, G., Du, X., Chen, D., Huang, Q., 2022. Sequential combined adsorption and solid-phase photocatalysis to remove aqueous organic pollutants by H_3PO_4-modified TiO_2 nanoparticles anchored on biochar. J. Water Process. Eng. 45, 102467. http://dx.doi.org/10.1016/j.jwpe.2021.102467.

Song, H., Wu, R., Yang, J., Dong, J., Ji, G., 2018. Fabrication of CeO_2 nanoparticles decorated three-dimensional flowerlike BiOI composites to build p-n heterojunction with highly enhanced visible-light photocatalytic performance. J. Colloid Interface Sci. 512, 325–334. http://dx.doi.org/10.1016/j.jcis.2017.10.080.

Song, J., Zhang, J., Zad, A., Ma, Y., Qi, K., 2023. $CoFe_2O_4$/$NiFe_2O_4$ S-scheme composite for photocatalytic decomposition of antibiotic contaminants. Ceram. Int. 49, 12327–12333. http://dx.doi.org/10.1016/j.ceramint.2022.12.088.

Sudhaik, A., Raizada, P., Ahamad, T., Alshehri, S.M., Nguyen, V.H., Le, Q.V., Thakur, S., Thakur, V.K., Selvasembian, R., Singh, P., 2023. Recent advances in cellulose supported photocatalysis for pollutant mitigation: A review. Int. J. Biol. Macromol. 226, 1284–1308. http://dx.doi.org/10.1016/j.ijbiomac.2022.11.241.

Sun, X., Li, Y., Du, Y., Li, Z., Jiang, N., Qu, J., Xue, L., Sun, G., 2021. In situ construction of $Bi_4O_5I_2$-$Bi_2O_2CO_3$-BiOCl $_{0.8}I_{0.2}$ n-p-n heterojunction for enhanced photocatalytic performance. Colloids Surf. A Physicochem. Eng. Asp 626, 126988. http://dx.doi.org/10.1016/j.colsurfa.2021.126988.

Sun, M., Yao, Y., Ding, W., Anandan, S., 2020. N/Ti^{3+} co-doping biphasic TiO_2/Bi_2WO_6 heterojunctions: Hydrothermal fabrication and sonophotocatalytic degradation of organic pollutants. J. Alloys Compd. 820, 153172. http://dx.doi.org/10.1016/j.jallcom.2019.153172.

Taddesse, A.M., Alemu, M., Kebede, T., 2020. Enhanced photocatalytic activity of p-n-n heterojunctions ternary composite Cu_2O/ZnO/Ag_3PO_4 under visible light irradiation. J. Environ. Chem. Eng. 8, 104356. http://dx.doi.org/10.1016/j.jece.2020.104356.

Thambiliyagodage, C., 2022. Efficient photocatalysis of carbon coupled TiO_2 to degrade pollutants in wastewater–A review. Environ. Nanotechnol. Monit. Manag 18, 100737. http://dx.doi.org/10.1016/j.enmm.2022.100737.

Vaya, D., Surolia, P.K., 2020. Semiconductor based photocatalytic degradation of pesticides: An overview. Environ. Technol. Innov. 20, 101128. http://dx.doi.org/10.1016/j.eti.2020.101128.

Vigneshwaran, S., Jun, B.M., Prabhu, S.M., Elanchezhiyan, S.S.D., Ok, Y.S., Meenakshi, S., Park, C.M., 2020. Enhanced sonophotocatalytic degradation of bisphenol a using bimetal sulfide-intercalated MXenes, 2D/2D nanocomposite. Sep. Purif. Technol. 250, 117178. http://dx.doi.org/10.1016/j.seppur.2020.117178.

Wang, S., An, W., Lu, J., Liu, L., Hu, J., Liang, Y., Cui, W., 2022d. A Cu/$CuFe_2O_4$-OVs two-electron centre-based synergistic photocatalysis-Fenton system for efficient degradation of organic pollutants. Chem. Eng. J. 441, 135944. http://dx.doi.org/10.1016/j.cej.2022.135944.

Wang, X., Li, Z., Zhang, Y., Li, Q., Du, H., Liu, F., Zhang, X., Mu, H., Duan, J., 2022b. Enhanced photocatalytic antibacterial and degradation performance by p-n-p type $CoFe_2O_4$/$CoFe_2S_4$/$MgBi_2O_6$ photocatalyst under visible light irradiation. Chem. Eng. J. 429, 132270. http://dx.doi.org/10.1016/j.cej.2021.132270.

Wang, X., Ma, J., Kong, Y., Fan, C., Peng, M., Komarneni, S., 2019a. Synthesis of p-n heterojunction Ag_3PO_4/$NaTaO_3$ composite photocatalyst for enhanced visible-light-driven photocatalytic performance. Mater. Lett. 251, 192–195. http://dx.doi.org/10.1016/j.matlet.2019.05.078.

Wang, F., Ma, N., Zheng, L., Zhang, L., Bian, Z., Wang, H., 2022a. Interface engineering of p-p Z-scheme BiOBr/$Bi_{12O17Br2}$ for sulfamethoxazole photocatalytic degradation. Chemosphere 307, 135666. http://dx.doi.org/10.1016/j.chemosphere.2022.135666.

Wang, C., Ni, H., Dai, J., Liu, T., Wu, Z., Chen, X., Dong, Z., Qian, J., Wu, Z., 2022c. Comparison of highly active Type-I and Type-II heterojunction photocatalytic composites synthesized by electrospinning for humic acid degradation. Chem. Phys. Lett. 803, 139815. http://dx.doi.org/10.1016/j.cplett.2022.139815.

Wang, H., Quan, X., Xiong, Q., Yin, L., Tian, Y., Zhang, J., 2023. Enhanced performance of β-cyclodextrin modified Cu_2O nanocomposite for efficient removal of tetracycline and dyes: Synergistic role of adsorption and photocatalysis. Appl. Surf. Sci. 621, 156735. http://dx.doi.org/10.1016/j.apsusc.2023.156735.

Wang, Y., Zhang, A., Zhang, D., Zhou, P., Wang, R., Xiang, J., Zhang, X., Su, S., 2019b. Ag_2CO_3 anchored on $BiOI/CoFe_2O_4$ composites with p-n-p heterojunctions: Highly enhanced activity for photocatalytic oxidation of Hg^0 under fluorescent light irradiation. Colloids Surf. A Physicochem. Eng. Asp 579, 123654. http://dx.doi.org/10.1016/j.colsurfa.2019.123654.

Wei, J., Shen, W., Liu, Y., 2023. Facile synthesis of $SrWO_4$@MIL-88A(Fe) heterojunctions and their deep treatment of dye wastewater and municipal landfill leachate using photo-Fenton technology. J. Ind. Eng. Chem. 120, 103–120. http://dx.doi.org/10.1016/j.jiec.2022.12.014.

Wu, Y., Gao, Z., Jiao, S., Zhou, G., 2023. Piezo-photo coupling effect and extended optical absorption of piezoelectric-based hybrids for efficient bisphenol a degradation. Chem. Eng. J. 452, 139456. http://dx.doi.org/10.1016/j.cej.2022.139456.

Xiang, D., Lu, S., Ma, Y., Zhao, L., 2022. Synergistic photocatalysis-Fenton reaction of flower-shaped CeO_2/Fe_3O_4 magnetic catalyst for decolorization of high concentration congo red dye. Colloids Surf. A Physicochem. Eng. Asp 647, 129021. http://dx.doi.org/10.1016/j.colsurfa.2022.129021.

Xu, R., Li, J., Sui, G., Zhuang, Y., Guo, D., Luo, Z., Liang, S., Yao, H., Wang, C., 2023. Construction of novel CdS@CuS/g-C_3N_4 heterojunctions for efficient visible light-driven photo-Fenton degradation performance. Colloids Surf. A Physicochem. Eng. Asp 659, 130598. http://dx.doi.org/10.1016/j.colsurfa.2022.130598.

Yahia, B., Faouzi, S., Ahmed, C., lounis, S., Mohamed, T., 2022. New hybrid process for amoxicillin elimination by combination of adsorption and photocatalysis on (CuO/AC) under solar irradiation. J. Mol. Struct. 1261, 132769. http://dx.doi.org/10.1016/j.molstruc.2022.132769.

Yang, B., Guan, B., 2022. Synergistic catalysis of ozonation and photooxidation by sandwich structured MnO_2-NH_2/GO/p-C_3N_4 on cephalexin degradation. J. Hazard. Mater. 439, 129540. http://dx.doi.org/10.1016/j.jhazmat.2022.129540.

Yang, Q., Li, X., Tian, Q., Pan, A., Liu, X., Yin, H., Shi, Y., Fang, G., 2023. Synergistic effect of adsorption and photocatalysis of BiOBr/lignin-biochar composites with oxygen vacancies under visible light irradiation. J. Ind. Eng. Chem. 117, 117–129. http://dx.doi.org/10.1016/j.jiec.2022.09.044.

Yin, G., Fu, C., Zhang, F., Wu, T., Hao, S., Wang, C., Song, Q., 2023. Piezocatalytic degradation of organic dyes and production of H_2O_2 with hydroxyapatite. J. Alloys Compd. 937, 168382. http://dx.doi.org/10.1016/j.jallcom.2022.168382.

Yu, Y., Hu, X., Li, M., Fang, J., Leng, C., Zhu, X., Xu, W., Qin, J., Yao, L., Liu, Z., Fang, Z., 2022. Constructing mesoporous Zr-doped SiO_2 onto efficient Z-scheme TiO_2/g-C_3N_4 heterojunction for antibiotic degradation via adsorption-photocatalysis and mechanism insight. Environ. Res. 214, 114189. http://dx.doi.org/10.1016/j.envres.2022.114189.

Yu, Y., Huang, H., 2023. Coupled adsorption and photocatalysis of g-C_3N_4 based composites: Material synthesis, mechanism, and environmental applications. Chem. Eng. J. 453, 139755. http://dx.doi.org/10.1016/j.cej.2022.139755.

Zhang, X., Chen, Z., Li, X., Wu, Y., Zheng, J., Li, Y., Wang, D., Yang, Q., Duan, A., Fan, Y., 2023. Promoted electron transfer in Fe^{2+}/Fe^{3+} co-doped $BiVO_4/Ag_3PO_4$ S-scheme heterojunction for efficient photo-Fenton oxidation of antibiotics. Sep. Purif. Technol. 310, 123116. http://dx.doi.org/10.1016/j.seppur.2023.123116.

Zheng, R., Yang, D., Chen, Y., Bian, Z., Li, H., 2022. Fe_2O_3/TiO_2/reduced graphene oxide-driven recycled visible-photocatalytic fenton reactions to mineralize organic pollutants in a wide pH range. J. Environ. Sci. http://dx.doi.org/10.1016/j.jes.2022.01.042.